UNIVERSITÀ
DI TORINO

University of Turin

Department of Molecular Biotechnology and Health Sciences

Molecular Medicine Ph.D. Program

XXXVI cycle

RICTOR/mTORC2 downregulation in BRAF^{V600E} melanoma cells promotes resistance to BRAF/MEK inhibition

Candidate

Ponzone Luca

Supervisor

Prof. Vincenzo Calautti

Co-supervisor

Prof.ssa Federica Cavallo

TABLE OF CONTENTS

Abstract

The main drawback of BRAF/MEK inhibitors (BRAF/MEKi)-based targeted therapy in the management of BRAF-mutated cutaneous metastatic melanoma is the development of therapeutic resistance. Thus, identification of prognostic markers of targeted therapy resistance is of pivotal importance. We aimed to assess in this context the role of mTORC2, a signaling complex defined by the presence of the essential RICTOR subunit, regarded as an oncogenic driver in several tumor types, including melanoma.

We interrogated The Cancer Genome Atlas (TCGA) melanoma patients' database to explore both overall survival and molecular signatures as a function of intra-tumor RICTOR levels and found that low RICTOR levels in BRAF-mutated melanomas correlate with a worse clinical outcome. Gene Set Enrichment Analysis of low-RICTOR tumors display gene signatures suggestive of activation of the mitochondrial Electron Transport Chain (ETC) energy production.

In vitro analysis showed that RICTOR-deficient $BRAF^{V600E}$ cells are intrinsically tolerant to BRAF/MEKi and anticipate the onset of resistance to BRAFi upon prolonged drug exposure. Moreover, in drug-naïve cells we observed a decline in RICTOR expression shortly after BRAFi exposure.

Proteomic screening aimed to identify proteins modulated by changes in RICTOR expression identified alterations in several proteins involved in mitochondrial metabolism and NAD^+ biosynthetic processes. We found that in RICTOR-depleted cells, both mitochondrial respiration and expression of nicotinamide phosphoribosyltransferase (NAMPT) are enhanced, and the combination of BRAFi with drugs targeting NAMPT or ETC restores the sensitivity of RICTOR-deficient cells *in vitro* and in a xenograft setting *in vivo*.

Our work unveils an unforeseen tumor-suppressing role for mTORC2 in the early adaptation phase of $BRAF^{V600E}$ melanoma cells to targeted therapy and identifies the NAMPT-ETC axis as a potential therapeutic vulnerability of low RICTOR tumors. Importantly, our findings indicate that the evaluation of intra-tumor RICTOR levels has a prognostic value in metastatic melanoma and may help to guide therapeutic strategies in a personalized manner.

1.1 Clinical management of metastatic melanoma

Even though it accounts for about 1% of all skin tumors, malignant melanoma is the most aggressive and deadliest form of skin cancer. Melanoma cases have been on the rise in the last few years and represent the 5th most common type of tumor(1). Most common risk factor associated with melanoma is UV exposure, while other factors increasing the chances to develop melanoma are white skin, family history, tendency to freckle, large number of nevi and immunosuppression(2). More than 50% of melanoma cases are driven by mutations on BRAF proto-oncogene, of which ~90% are represented by V600E mutation(3,4). This type of mutation renders the protein constitutively active even in the absence of extracellular stimuli, engaging in constitutive activation of Mitogen Activated Protein Kinase (MAPK) pathway and ultimately leads to uncontrolled proliferation of melanoma cells(5).

Surgical resection is always recommended when feasible, with neoadjuvant therapy suggested for stage IIIB/IV and adjuvant therapy suggested after resection. Until relatively recent years, pharmacological treatment of melanoma involved radiotherapy, high-dose Interleukin-2 (IL-2) and the chemotherapeutic agent Dacarbazine(6).

The last two decades saw a marked increase in melanoma patients' survival thanks to the clinical introduction of MAPK inhibitors-based targeted therapy (TT) and more recently Immune Checkpoint Inhibitors (ICI).

1.1.1 Introduction of BRAF- and MEK-inhibitors

The need to find better therapeutical options lead to the development and subsequent clinical approval of BRAF inhibitors (BRAFi), a class of drugs that strongly and specifically target the mutated form of BRAF. One of the first developed BRAFi is Vemurafenib (PLX4720), which specifically targets the V600E/K mutations, and which was approved by FDA in 2011 after a Phase-III study by Chapman and colleagues(7). This study compared the efficacy of single-agent Vemurafenib against Dacarbazine, showing a 6-months overall survival of 84% in Vemurafenib compared to 64% of chemotherapy, with a 74% reduction in the risk of death or disease progression(7). After Vemurafenib, other BRAFi were approved as therapeutic agents, like Dabrafenib in 2013(8,9) and Encorafenib in 2018(10).

While clinical introduction of BRAFi significantly improved the overall survival of melanoma patients carrying BRAF mutations, long-term remissions were still relatively rare due to toxicity and to the arise of drug resistance. BRAFi toxicity concerns have important implications that may limit their use and need to be taken into account in clinical settings. Toxicity to BRAFi results from both on-target and off-target effects, with off-targets specifically depending on the molecule(11,12), while on-target side-effects are mainly due to paradoxical activation of MAPK pathway in non-cancerous tissues. This happens as a consequence of increased formation BRAF/CRAF dimers, which can still activate MAPK pathway(13), and in some cases this may lead to the development of other malignancies like keratoacanthoma and squamous cell carcinoma(14,15), which may be limited by concomitant treatment with MEK inhibitors (MEKi).

Other than therapy-induced adverse effects, BRAFi efficacy is limited by the development of therapeutic resistance in a large portion of patients (discussed more in detail in section 1.2), which emerges also in melanomas that initially respond well to BRAFi. Resistance to targeted therapy often involves reactivation of downstream MAPK pathway and combination with MEKi is now used as frontline therapy in order to delay the insurgence of resistance to BRAFi(16,17).

BRAF/MEKi (Dabrafenib + Trametinib) combination was approved for clinical use for the first time in 2014 following the publication of phase I-II study by Flaherty et al. and a phase III study by Robert et al., and in later years other BRAF/MEKi combinatorial regimens were approved (Vemurafenib + Cobimetinib in 2015, Encorafenib + Binimetinib in 2018). Unfortunately, while BRAF/MEKi combination increases the progression-free survival of BRAF-mutated melanoma patients, drug resistance is still a major concern. Several features that characterize targeted-therapy resistant melanomas have been identified during the years, but we still lack reliable markers that could predict the outcome of BRAF/MEKi therapy. Identifying markers of early development of drug resistance could help directing melanoma patients to alternative therapeutic strategies, such as Immunotherapy or combination with other FDA-approved drugs.

1.1.2 Immunotherapy

Immunotherapeutic approaches aim at activating the patient's immune cells, instructing them to target and eliminate cancer cells. Immunotherapy comprises different approaches like the use of Immune Checkpoint Inhibitors (ICI), oncolytic viruses, Chimeric Antigen Receptor (CAR) T-cells and cancer vaccines. ICI work by blocking inhibitory pathways of immune cells that are exploited by cancers to escape immune clearance and clinical introduction of ICI brought novel and effective alternative for the treatment of tumors. First approved ICI was the anti-PD-1 antibody Ipilimumab in 2011, while other antibodies against PD-1 or other Immune checkpoints (CTLA-4, PD-L1) have been approved in the following years (**Fig 1A**).

Considering the mechanism of action, ICI can be used for the treatment of many types of tumors, even though highest efficacy has been shown in non-small cell lung cancer, renal cell carcinoma, bladder cancer and especially in melanomas(18). Compared to BRAF/MEKi, immunotherapy regimens could be extended also to patients driven by different mutations other than BRAF. Nonetheless, not all patients benefit from treatment with ICI and an important amount of research is being conducted on this field, leading to a deeper understanding of mechanisms which regulate immune evasion. Immune-related adverse events can be severe ad long-lasting, with uncommon occurrence of lethal events(19,20). Frequency and severity of adverse effects have been researched by different studies and their clinical management often involves immune-suppressing regimens.

Furthermore, evidence supports the presence of common mechanisms that drive resistance to both targeted therapy and ICI(21), leading to the development of cross-resistance between these two approaches. Thus, a more complete understanding of the events happening and driving

acquisition of TT resistance may shed light also on the mechanisms underlying unresposivness to ICB.

1.2 Targeted-therapy resistance in melanoma

Since their clinical introduction, targeted therapy approaches have their major drawback in the development of therapeutic resistance. Unresponsiveness to TT may be put in different categories depending on the timing of onset. For example, drug-naïve cancer cells that possess *a priori* features that grant them resistance are defined as “intrinsically” resistant, while tumors that underwent genetic changes driven by prolonged exposure to BRAF/MEKi have features of “acquired resistance”. Moreover, melanomas that initially respond to TT but gradually become unresponsive can present reversible changes and are in a phase of “adaptive resistance”. These categories of resistance present distinctive features that are often confined to one state or the other, but are similar for some aspects, sometimes blurring the strict distinction between adaptive and acquired resistance(16,17,22) (**Fig 1B**).

The most common feature that characterizes all TT resistance states is the incomplete inhibition of MAPK pathway in presence of BRAF/MEKi, which may be caused by engagement of signaling pathways parallel to MAPK, genomic amplification of BRAF or even the development of activating mutations on BRAF-downstream effectors like MEK.

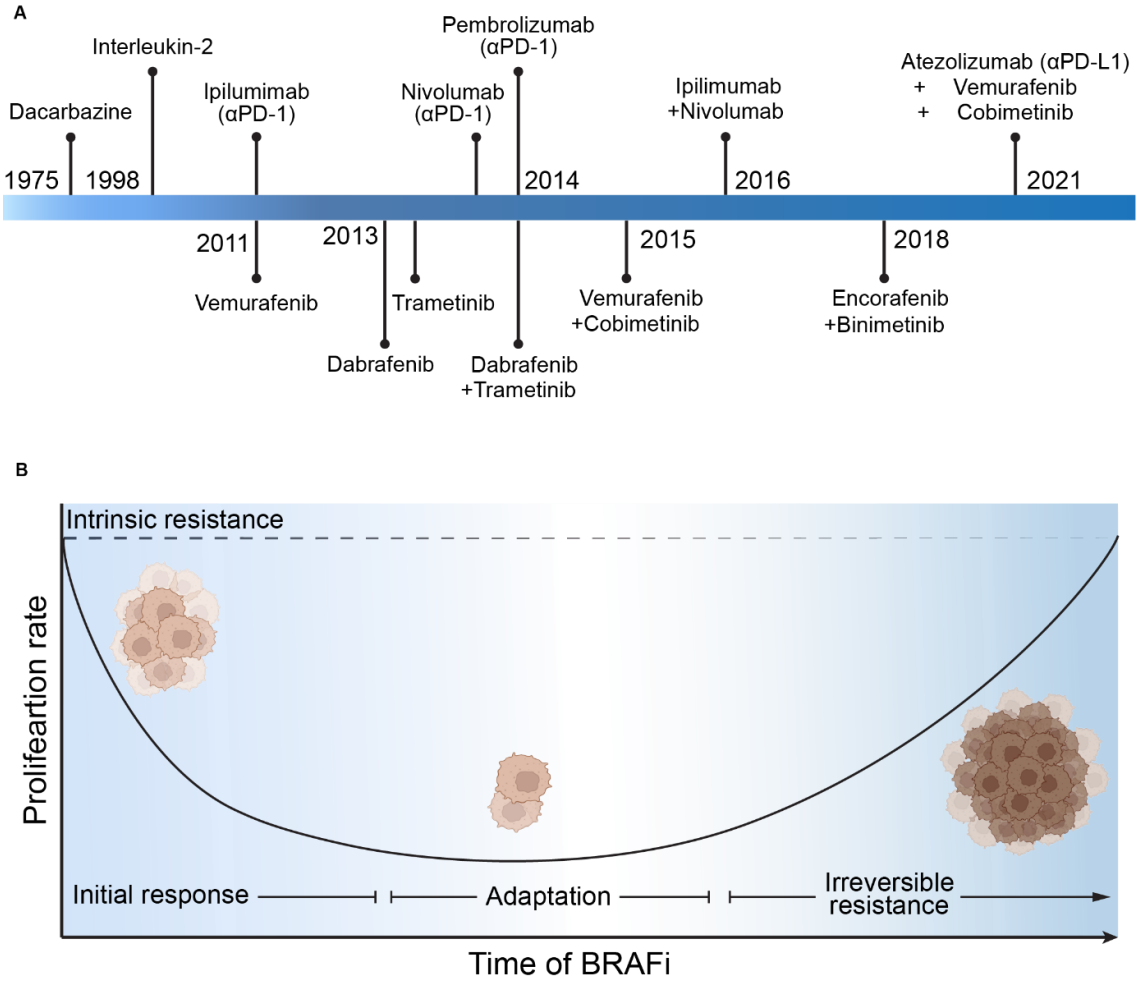

Figure 1 – Metastatic melanoma treatments and resistance acquisition. A) Timeline for FDA-approved therapies for metastatic melanoma **B)** Schematic representation of targeted-therapy resistance mechanism of melanoma

1.2.1 Intrinsic resistance

A fraction of $BRAF^{V600E}$ melanomas (around 20%(16)) do not respond to BRAFi even in the first phases of drug exposure. These cancer cells are defined as “intrinsically resistant” and their occurrence may be caused by different mechanisms, which often involve mutational events affecting MAPK and PI3K/Akt pathways. For example, loss of tumor suppressor PTEN activates Akt signaling and correlates with reduced response to targeted therapy in BRAF-mutated melanoma cell lines(23). Moreover, PTEN reduction or loss has been shown to promote progression and therapeutic resistance in melanoma and other types of cancer(24).

Another tumor suppressor often lost in melanoma is NF-1 (about 13% of all melanomas), a RAS GTPase activating protein that negatively regulates MAPK pathway. NF-1 loss has been shown to promote melanoma development(25) and NF-1 alterations are found in melanoma cells intrinsically resistant to BRAF inhibitors (26,27)

Other common mutations that grant enhanced intrinsic resistance and proliferation potential to melanoma cells may involve RB and RAC1 pathways. Specifically, p16 loss of function may originate by deletions and inactivating mutations, and cyclin D1 gene is amplified in almost 20% or $BRAF^{V600E}$ melanomas(28). Moreover, RAC1 is the third most common hotspot mutation(29,30).

1.2.2 Adaptive and acquired resistance

Prolonged exposure to targeted therapy (weeks or months of continuous treatment) can lead to development of therapeutic resistance in previously sensitive cells, due to the emergence of novel alterations and mutations. These mechanisms are of diverse nature and generally the first phases of resistance acquisition involve metabolic and epigenetic changes, while genomic mutations appear later.

Metabolic rewiring and epigenetic landscape are not irreversible and can be changed back to the sensitive state by suspending drug treatment, thus sensitizing again drug-exposed cancer cells. Instead, TT-driven mutations cannot be reverted by suspending drug treatment and are at the basis of hardwired resistance status.

Microphtalmia-associated transcription factor (MITF) is a master regulator that controls many processes of melanoma cells including invasion, survival and cell cycle(31,32), and changes in MITF levels are found in different steps of TT-resistance acquisition. For example, there is evidence that BRAFi treatment causes an increase of MITF levels which are connected to drug tolerance and resistance acquisition(32). On the other hand, other works identified MITF-low subpopulations as more invasive and resistant to targeted therapy(31,33).

Moreover, BRAFi exposure modifies the cellular energetic metabolism and drug-resistant cells show a switch from a glycolysis-based metabolism to an OXPHOS-dependent one. This metabolic reprograming can be induced by acute treatment with BRAF/MEKi though different mechanisms, involving mitochondrial functions directly or indirectly.

Constant treatment with MAPKi applies selective pressure on the newly develop mutations, preserving and expanding the ones that grant increased fitness in the presence of the drugs. Interestingly, some mutations positively selected by the drugs can be deleterious in the absence of the inhibitors and this phenomenon ca be exploited in a clinical setting, by discontinuing the drugs and sensitizing again the cells.

1.2.3 Metabolic rewiring

Cancer cells possess high metabolic plasticity widely recognized as one of the hallmarks of cancer(34–36). Tumors are able to dynamically adapt their metabolism to the nutrient restriction and changes, acidity, hypoxic conditions, and cell–cell interactions within the TME(37–39).

The first phenomenon of metabolic adaptation described to happen in cancer is the Warburg effect, according to which tumor cells do not take advantage of the mitochondrial oxidative

phosphorylation (OXPHOS) to produce energy, but show high rates of glucose uptake and lactate secretion, even in the presence of oxygen (i.e., aerobic glycolysis)(40–42). It is now clear that aerobic glycolysis/Warburg effect is not the only metabolic pathway used by cancer cells to sustain their growth. Rather, mitochondrial metabolism emerged as a crucial player in promoting malignant transformation(43). Mitochondria produce most of the ATP needed to sustain cellular processes, but also function as stress sensors and are responsible for the adaptation of the cell to environmental conditions. Despite their physiological roles, mitochondria can also contribute to tumorigenesis and cancer progression producing high levels of reactive oxygen species (ROS), metabolites driving the accumulation of DNA mutations and the activation of oncogenic signaling pathways, and regulate antigen presentation to immune cells(43–46).

However, the metabolic flexibility of cancer cells is very complex and comprises several pathways. Cancer cells compensate for glucose deprivation by increasing amino acids scavenging and uptake of different molecules (glutamine, fatty acids and acetate) which will then be converted in order to ensure the continuous supply of nutrients(35,39).

In the early stages of development melanoma cells metabolize up to 80% of glucose into lactate (showing classical Warburg phenotype), and the following hypoxic conditions potentiate this metabolic process(47,48). Lactate and protons secretion due to the overactivation of glycolysis drastically alters the melanoma microenvironment, facilitating angiogenesis, promoting melanoma metastasis, and suppressing the immune system(49). BRAF oncogenic signaling has emerged as a critical regulator of this metabolic pathway in melanoma as MAPK pathway activates transcription factors, such as MYC and hypoxia inducible factor-1α (HIF-1α), which are key regulators of glycolysis(42,50). In parallel, BRAF mutations can block OXPHOS, repressing expression of MITF and its target PGC-1α(51,52). Acute treatment with BRAFi and MEKi rapidly reduces glucose uptake and inhibits the glycolytic pathway, both *in vitro* and *in vivo*(53,54). Melanoma cells attempt to survive under drug's pressure switching from glycolysis to a mitochondrial metabolism(51). In general, this is obtained through enhancement of mitochondrial activity and mitochondrial content reactivating the MITF/PCG-1α axis(51,52,55). However, it is noteworthy that melanoma is a highly heterogeneous tumor, and subsets of melanoma possess an oxidative metabolism, correlating with poorer survival, progression, and metastasis. Thus, both glycolysis and OXPHOS play a significant role in metabolic rewiring of melanoma cells, and there is a dynamic switch and plasticity between these two metabolic phenotypes(48,56).

This adaptive metabolic program limits the efficacy of targeted-therapy and is one of the mechanisms responsible for adaptive resistance(51,55). Another important factor that regulates metabolic plasticity is the maintenance of appropriate NAD levels, which are critical to maintain redox reactions and generate adequate energy, as well as to sustain NAD-consuming enzyme activities (i.e., mono and poly-ADP-ribose polymerases (ARTs, PARPs), CD38/CD157 and sirtuins), orchestrating fundamental biological processes like DNA repair, apoptosis, gene expression, transcription, immune regulation and cell cycle progression(57,58). In tumors, many of these processes are de-regulated and thus a fine-tuned regulation of NAD levels is a critical

element during malignant transformation and progression(57,59). NAD homeostasis is the result of a dynamic balance between its biosynthesis and consumption, and cells maintain adequate NAD levels through multiple biosynthetic enzymatic pathways. However, a common strategy of several tumors is to sustain NAD production over-expressing its rate-limiting and vital enzyme NAMPT that converts the NAD precursor nicotinamide in nicotinamide mononucleotide (NMN), as first step in NAD regeneration(57). Therefore, NAMPT is a critical factor involved in the modulation of cellular metabolism but also signaling pathways(60–62).

Thus, metabolic dependencies of cancer cells on alternative nutrients to support energy production may offer opportunities for the development of novel targeted therapies to hit multiple tumor vulnerabilities.

1.3 mTOR and its complexes

mTOR is a serine/threonine protein kinase belonging to the phosphatidylinositol 3-kinase-related kinases (PIKK) family and nucleates at least two multi-protein complexes, namely mTOR complex-1 (mTORC1) and mTOR complex-2 (mTORC2). The two mTOR-containing complexes have distinct roles and regulate a plethora of biological processes, such as cell growth, proliferation, protein and lipid synthesis, cancer, aging, lysosome biogenesis, immune modulation, and stress response.

mTORC1 is composed of five protein subunits (including mTOR): two subunits shared with mTORC2, namely mLST8 (mammalian lethal with Sec13 protein 8)(63) and DEPTOR (DEP-domain-containing mTOR-interacting protein)(64), and two exclusive subunits, Raptor (regulatory-associated protein of mTOR){Citation} and PRAS40 (proline-rich Akt substrate 40 kDa)(65). The presence of growth factors and nutrients (such as amino acids) promotes mTORC1-dependent protein synthesis through phosphorylation of two key protein substrates: 4E-BP1, which then dissociates from eIF4E, leading to initiation of protein translation, and S6K1 protein kinase.

Upstream signaling by amino acids leads to localization of mTORC1 at the lysosomal surface, where it becomes activated by GTP-bound Rheb(66). The amount of GTP-bound, active Rheb is negatively regulated by the GAP activity of tuberous sclerosis-1 and -2 (TSC1/TSC2) protein complexes that stimulate the intrinsic GTPase activity of the protein. Phosphorylation by Akt and ERKs of TSC complexes leads to their inactivation and, thus, promotes the accumulation of the GTP-bound form of Rheb with subsequent activation of mTORC1 at the lysosomal surface. Both growth factors and nutrients converge on the activation of mTORC1 and starvation acts as a physiological inhibitor of this signaling complex, together with different forms of cellular stress(67,68).

Sustained mTORC1 activation induces negative feedback mechanisms that desensitize cells to growth-factors-dependent stimuli, for example through S6K1-dependent degradation of the IRS1 adaptor protein(68).

mTORC2 complex is composed of mTOR, mLST8, DEPTOR, Sin1/MAPKAP1 (mammalian stress-activated MAPK-interacting protein 1), Rictor (rapamycin-insensitive companion of mTOR), and Protor1/2 (protein observed with Rictor 1/2) [239]. The best established function of this complex is the phosphorylation of AGC kinases, such as Akt/PKB, SGK1 (serum/glucocorticoid-regulated kinase 1), and PKCα (and possibly other PKC isoforms). Like mTORC1, mTORC2 is also involved in the regulation of cell metabolism in several tissues by promoting glycolysis, lipid synthesis, and amino acid transport(68).

1.3.1 mTORC2

mTORC2 phosphorylates Akt at Serine 473, located in the hydrophobic regulatory motif, which leads to full Akt kinase activation. Akt regulates cell survival, proliferation, and energetic metabolism via multiple protein substrates, such as TSC2, GSK3β (glycogen synthase kinase 3β), and FoxO proteins. SGK1 regulates ion transport and apoptosis(69), while PKCα controls cytoskeleton organization and cell motility(70).

mTORC2 regulation is primarily achieved by growth factor signaling through the PI3K pathway. The link between growth factor signaling, PI3K, and mTORC2 is provided by its integral component, Sin1, which possesses a pleckstrin homology domain that inhibits mTORC2 in the absence of active PI3K signaling. Binding to PI3K lipid products phosphatidyl inositol (3,4,5) triphosphate (PIP3) at the plasma membrane releases this inhibition and fosters interaction between mTORC2 and its Akt protein substrate, which is also recruited at PIP3-enriched membrane domains. Cross-phosphorylation between Akt and mTORC2 further modulates their activation and subcellular distribution(71,72). Interestingly, distinct subcellular pools of mTORC2 at the plasma membrane, mitochondria, and endosomal vesicles have been described, which possess a differential dependence on growth factor signaling and PI3K activity (reviewed in (73)).

1.3.2 mTORC2 in cancer and resistance

Activation of mTOR/Akt signaling is likely to occur during the development of nevi, which initially undergo a transient cell proliferation rapidly followed by growth arrest, via mechanisms reminiscent of the process of oncogene-induced senescence. The idea that mTOR activation plays essential roles in melanomagenesis is also strongly supported by work on murine melanoma models(4,74,75). Animals with a conditional expression of $BRAF^{V600E}$ in melanocytes develop benign melanocytic lesions reminiscent of human melanocytic nevi; concomitant loss of PTEN activates the PI3K/Akt/mTOR signaling, overcomes senescence induced by MAPK signaling and results in melanoma formation with 100% penetrance(76). The deletion of CDKN2A, a mutation that frequently occurs in all known melanoma genetic subtypes, was found associated with the activation of mTORC2/Akt signaling although the precise mechanisms underlying this event where not fully elucidated(76). In the context of $BRAF^{V600E}$ mutation, the

concomitant activation of both mTORC1 and mTORC2 can also be obtained by PTEN deletion. The involvement of mTORC2 in melanoma progression has been further suggested by the observation that the gene of its essential component Rictor is amplified in a subset of human melanomas(29). However, pan-cancer analysis of publically available datatets evidences that in specific tumors RICTOR may play an opposite role, particularly in glioma, melanoma and kidney carcinoma(77).

As previously described, the shift between glycolytic-based to OXPHOS mitochondrial energetic metabolism is a frequent feature in a substantial proportion of targeted-therapy resistant melanomas.

Transformed cells that are addicted to mTORC2 signaling have been found to depend on mitochondrial functions(78). On the other hand, mTORC2 is a positive regulator of glycolysis and lipid biogenesis via both Akt dependent and independent mechanisms (for review see (79)). However, in different cell types and tissues, mTORC2 deficiency induced by Rictor conditional ablation was found associated with an OXPHOS gene expression signature(80), with increased mitochondrial functions(81) and with increased glutamine consumption through the glutaminolytic pathway(82,83). Thus, it seems likely that, in melanoma, changes in the overall scenario induced by therapeutic regimens, modifications in the tumor microenvironment or acquisition of additional genetic alterations likely direct mTORC1 and mTORC2 on different subsets of downstream targets and cellular bioenergetics processes during the progression of BRAF-mutated melanoma towards therapeutic resistance. This picture is further complicated by the coexistence within the same tumor of cell populations with different bioenergetic needs and metabolic profiles. Very recent work suggests that post-transcriptional regulation of metabolic genes following BRAF inhibition plays a central role in the adaptation of $BRAF^{V600E}$ melanoma cells via translational reprogramming.

Thus, considering the key roles of mTORC2 in the regulation of cell metabolism, proliferation and survival, it is likely that this signaling complex may be involved in adaptive mechanisms of resistance to targeted therapy.

RESULTS

2.1 Low RICTOR levels correlate with poor prognosis in melanoma

To investigate the relationships between RICTOR expression and melanoma patients' survival, we interrogated the entire Skin Cutaneous Melanoma (SKCM) cohort of patients from the publicly available The Cancer Genome Atlas (TCGA) database with respect to overall survival (OS). No significant difference in RICTOR mRNA or protein expression was detected between BRAF-WT (n = 99) and -Mut (n = 93) tumors (**Fig 2A**). High RICTOR mRNA levels in metastatic tumors (367 out of 448 total samples) positively correlate with patients' survival, as indicated by a Kaplan-Meier curve obtained from patients falling in the first (n = 87) and fourth (n = 91) quartile of RICTOR expression (**Fig 2B**). This was also indicated by Cox regression analysis (p=0.007, median Hazard ratio = 0.68), using RICTOR expression as a continuous independent variable without imposing arbitrary thresholds (**Fig 2C**). In this analysis, however, no significant association with RICTOR mRNA expression and distinct genetic subtypes (BRAF-Mut, NF1-Mut, RAS-Mut, Triple WT) emerged. The positive correlation between RICTOR expression and patients' OS was also indicated by both Kaplan-Meyer and Cox analyses (p = 0.003, median Hazard ratio = 0.54) based on the TCGA protein dataset (**Fig 2D,E**). Kaplan-Meier analysis performed on BRAF-mutated (BRAF-Mut) tumors did not evidence significant correlations between survival and RICTOR mRNA levels (**Fig 2F**). However, both Kaplan-Meier and Cox analyses based on the TCGA protein expression dataset indicated significantly reduced survival in patients bearing BRAF-Mut tumors with low RICTOR expression (**Fig 2E,G**). Further analysis indicated that RICTOR mRNA is only moderately correlated (Pearson correlation = 0.384 and 0.335 respectively) with protein levels, and thus may not reliably reflect the corresponding protein level (**Fig 2H**).

Kaplan-Meyer and Cox analyses of the same cohort of patients stratified according to RAPTOR mRNA indicated that elevated levels of this essential mTORC1 component correlate with a shorter OS (**Fig 2I,J**), whereas the correlation between RAPTOR expression and patients' survival was not observable in the protein dataset (**Fig 2K**). No significant association with survival was found between MTOR levels and patients' survival (**Fig 2L,M**). Based on RICTOR and RAPTOR mRNA levels our data suggest that mTORC2 and mTORC1 may play opposite roles in melanoma progression and/or therapeutic responses.

Gene Set Enrichment Analysis (GSEA) revealed a significant anticorrelation between RICTOR expression levels and signatures relative to mitochondrial processes (e.g. Respiratory Electron transport chain; ATP Synthesis Coupled Proton Transport), coupled with stress protective and cell detoxifying pathways, both in the entire melanoma dataset as well as in the BRAF-Mut tumor subgroup (**Fig 2N,O**). Thus, low expression of RICTOR in metastatic melanoma is associated with a poor clinical outcome, and the gene expression signature of low RICTOR tumors indicates the activation of processes that are frequently associated with BRAF/MEKi resistance.

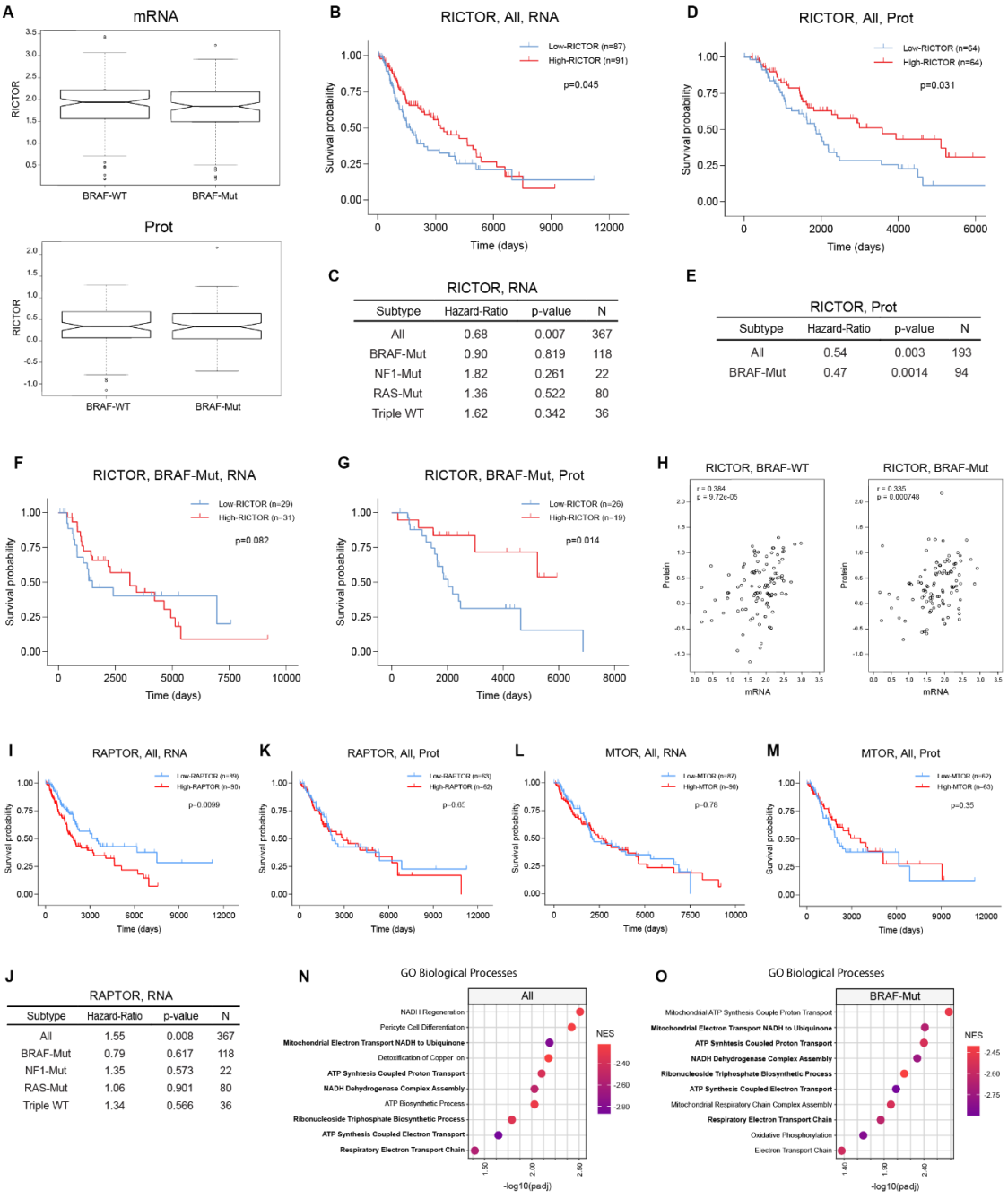

Figure 2 - Analysis of Melanoma patients' data from the TCGA database. A) Expression levels of RICTOR mRNA (*upper panel:* BRAF-WT n=138, BRAF-Mut n=118) and protein (*lower panel:* BRAF-WT n=99, BRAF-Mut n=94) in BRAF-WT and BRAF-Mut patients of the SKCM dataset. **B, D, F, G, I-M**) Kaplan-Meier (K-M) survival analyses of the metastatic Skin Cutaneous Melanoma (SKCM) dataset obtained from TCGA patients' database stratified depending on RICTOR/RAPTOR/MTOR expression. **C, E, J**) Cox regression analysis of the whole SKCM dataset (All) or after stratifying patients based on genetic subtypes (BRAF-Mut, NF1-Mut, RAS-Mut, Triple WT), using RICTOR/RAPTOR levels as continuous independent variables. "All" category also includes tumors for which information about the genetic subtype is not available and thus cannot be assigned to specific genetic subtypes. Number of patients (N), hazard-ratio and p-values calculated by likelihood ratio test are indicated for each subtype. **H**) Correlation analysis of RICTOR mRNA and protein levels in BRAF-WT (left panel) and BRAF-Mut (right panel) patients of the SKCM dataset. Pearson correlation coefficient (r) and p-value are indicated for each group (BRAF-WT n=99; BRAF-Mut n=94). **N,O**) Dotplots indicate the top 10 most significantly enriched Gene Ontology (GO) categories anticorrelated with RICTOR expression, in the (**H**) whole dataset (All; n = 367) or (**G**) after filtering for BRAF Hotspot Mutations (BRAF-Mut; n = 118). NES = Normalized Enrichment Score.

All = data obtained from analysis of the whole TCGA database irrespective of BRAF mutational status; RNA/Prot = data obtained from gene expression or Reverse Phase Protein Array (RPPA) data, respectively; High-RICTOR/RAPTOR =

fourth quartile; Low-RICTOR/RAPTOR = first quartile. Number of patients for each group and p-value calculated by Log-rank test are indicated in individual graphs.

2.2 Downregulation of RICTOR in BRAF^{V600E} melanoma cell lines promotes resistance to BRAF/MEKi

To establish whether RICTOR/mTORC2 downregulation affects the responses of melanoma cells to BRAFi-based targeted therapy, we stably silenced RICTOR in three BRAF-mutated human melanoma cell lines (M14, A375 and SK-MEL-28) via lentiviral delivery of two separate RICTOR-targeted shRNAs (shR1, shR2), and compared their effects with those of a scramble control shRNA (shC). Both RICTOR protein and mRNA levels were reduced, as well as the expression level of the other essential mTORC2 protein component SIN1(84)(**Fig 3A,B**). As readout of mTORC2 signaling activity, we monitored the phosphorylation levels of the downstream targets AKT and NDRG1 both under serum-deprived and -stimulated conditions. This analysis indicates that all the RICTOR-silenced cell lines display disruption of mTORC2 integrity and attenuation of downstream signaling, with no significant effects on proliferation rates under basal culture conditions (**Fig 3A**). Therefore, we used these cell lines as experimental models to investigate the effects of RICTOR/mTORC2 depletion in the response of BRAF-mutated melanoma cells to BRAF/MEKi.

Culture of BRAF-mutated melanoma cells in the presence of increasing concentrations of BRAFi can be used to generate BRAFi-resistant cell line variants from BRAFi-sensitive parental cells. We applied this procedure to evaluate the kinetics of acquisition of BRAFi-resistance in RICTOR-silenced and control cells of A375, M14 and SK-MEL-28 background over the course of ~ 8-9 weeks. We have arbitrarily set the experimental endpoint as the capacity of cells to expand in the presence of 1.6 μM Vemurafenib. Analysis of growth profiles of cell cultures in the presence of increasing drug concentrations showed that in all cellular backgrounds RICTOR-depleted cells anticipate by several weeks the reach of the experimental endpoint (**Fig 3C**). Interestingly, A375 shR1 acquired the resistance status earlier than shR2 variants, suggesting that within the same cellular background RICTOR levels correlate with the timing of resistance acquisition.

Growth assay showed that RICTOR silencing does not affect the basal proliferation rates of M14 or A375 cells (**Fig 3D**). To evaluate whether the anticipated acquisition of BRAFi resistance relies on an intrinsically higher tolerance to BRAFi of RICTOR-depleted cells, we have carried out Colony Formation Efficiency (CFE) survival assays by exposing M14 and A375 cells to fixed doses of BRAFi (Vemurafenib) and/or MEKi (UO126) over the course of 12 days. While RICTOR downregulation did not affect the basal proliferation rates or clonogenicity of cells, the results indicated that RICTOR-depleted cells are intrinsically more tolerant than RICTOR-proficient counterparts to BRAFi and their combination with MEKi (**Fig 3E**), as also confirmed by its acute siRNA-mediated downregulation (**Fig 3F,G**).

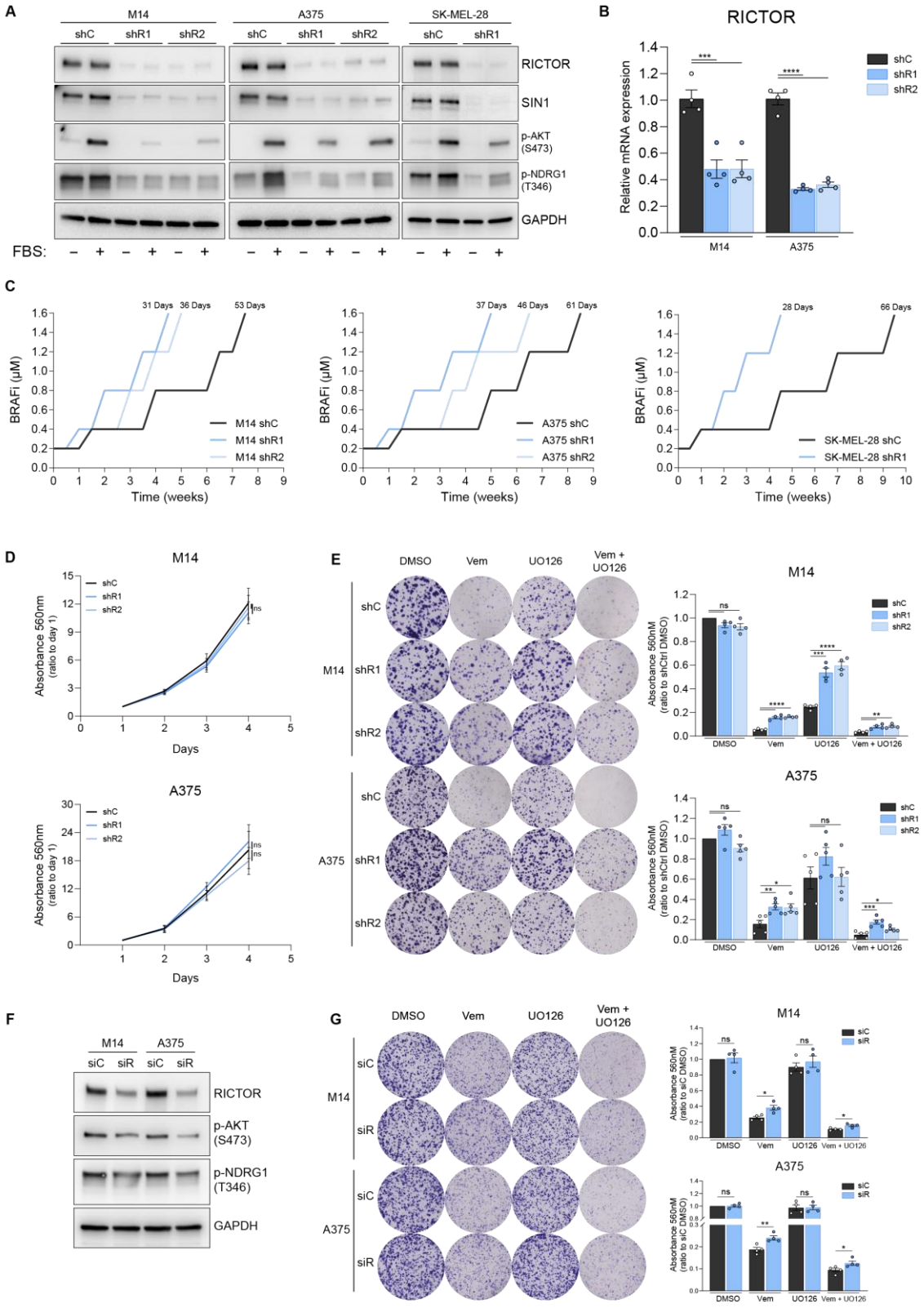

Figure 3 - Downregulation of RICTOR in BRAF^{V600E} melanoma cell lines promotes resistance to BRAF/MEKi. A) Western blot analysis of indicated cell lines transduced with RICTOR-targeting shRNAs (shR1, shR2) or scramble control (shC) lentiviruses. Cells were analyzed after 24 hours of serum starvation (-) or 24 hours of serum starvation followed by 15 minutes of refeeding (+). **B**) qRT-PCR analysis of RICTOR gene in indicated cell lines, bar graphs represent the mean values of 4 independent experiments ± SEM; ***p < 0.001, ****p < 0.0001, one-way ANOVA followed by Dunnett's multiple comparisons test. **C**) Resistance acquisition kinetics analysis of RICTOR-silenced (shR1, shR2) or control (shC) M14/A375/SK-MEL-28 cells exposed to increasing doses of BRAFi (Vemurafenib, from 0.2 to 1.6 μM). The number of

days required to reach resistance to 1.6 μM Vemurafenib is indicated on top of each curve. **D**) Proliferation assay performed on indicated cell lines, absorbance values are normalized on corresponding absorbance data at day 1. Curves represent the mean values of independent experiments (M14 N=6; A375 N=3) ± SEM. ns = not significant, one-way ANOVA followed by Dunnett's multiple comparisons test. **E**) Colony Formation Efficiency (CFE) assay of indicated cell lines cultured for 12 days in presence of vehicle control (DMSO), 0.5 μM Vemurafenib (Vem), 0.5 μM UO126 (UO126) or the combination of 0.5 μM Vemurafenib + 0.5 μM UO126 (Vem + UO126). Bar graphs represent the mean values of independent experiments ± SEM (n = 4 for M14 cells; n = 5 for A375 cells). ns = not significant, *p < 0.05, **p < 0.01, ***p < 0.001, ****p < 0.0001, one-way ANOVA followed by Dunnett's multiple comparisons test. **F**) Western blot analysis of indicated cell lines transfected with a RICTOR-targeting (siR) or Non-targeting control (siC) siRNAs at 72 hours after transfection. **G**) CFE assay of indicated cell lines cultured for 7 days in presence of DMSO, Vem, UO126 or the combination of Vem + UO126 as in **E**). Bar graphs represent the mean values of 4 independent experiments ± SEM. ns = not significant, *p < 0.05, **p < 0.01, unpaired t test.

2.3 RICTOR protein downregulation occurs as a consequence of MAPK inhibition

Because RICTOR levels affect the kinetics of acquisition of BRAFi resistance, it was important to determine whether the endogenous levels of the protein could be modulated in response to BRAF inhibition. Indeed, in drug-naïve M14, A375 and SK-MEL-28 cells the levels of RICTOR were significantly reduced by Vemurafenib treatment, paralleled by attenuated phosphorylation of the mTORC2 downstream target NDRG1 (**Fig 4A**). In M14 and SK-MEL-28 cells AKT phosphorylation at Ser473 decreased in parallel with RICTOR, whereas in A375 cells Vemurafenib exposure increased AKT phosphorylation. This uncoupling between RICTOR and phospho-AKT levels is consistent with previous evidence of alternative, mTORC2-independent mechanisms of AKT Hydrophobic motif phosphorylation(85–88) reported also to occur in BRAF-mutated melanoma cells, including A375(85). Vemurafenib-induced decrease in RICTOR protein levels were not matched by a parallel decrease in mRNA, suggesting a post-transcriptional mechanism of regulation (**Fig 4B**). Accordingly, concomitant treatment with proteasome inhibitor Bortezomib prevented BRAFi-induced RICTOR downregulation (**Fig 4C**).

As RICTOR-silenced cells display an advantage in clonogenic growth upon BRAF inhibition, we investigated how survival/proliferation pathways are modulated under these conditions as a function of RICTOR expression and BRAF inhibition. Visual inspection of cultures kept in presence of BRAFi over the course of 12 days confirmed that colonies that survive treatment were progressively expanding, as also evidenced by similar levels of phospho-RB proliferation marker between treated and untreated colonies (**Fig 4D**). Consistent with previous data, in drug naïve RICTOR-proficient cells the endogenous levels of RICTOR protein were significantly reduced in the presence of Vemurafenib. Although the colonies generated by RICTOR-deficient cells were more abundant and larger than those generated by control counterparts, we did not detect significant differences in the levels of ERK, AKT or RB phosphorylation that could account for their drug-tolerant phenotype (**Fig 4D**). These data suggest that RICTOR downregulation occurs during the initial response and early adaptation phase to BRAFi, that normally precede the development of further mechanisms typical of acquired drug resistance.

To shed light on the mechanisms in which RICTOR downregulation plays a role in the early adaptation of cells to BRAFi, we analyzed pathways previously implicated in BRAF/MEKi resistance in multiple melanoma cell lines. These include Receptor Tyrosine Kinase (AXL(31)),

transcriptional regulators (MITF, SOX10(31,32,89,90)) and BRAF downstream effectors (ERK, MEK, p-p90-RSK, RB(91,92)) as readout of MAPK signaling activation. Our analysis revealed that changes in RICTOR expression levels, either Vemurafenib- or shRNA-induced, did not correlate with modulation of MAPK signaling outputs nor with univocal changes in expression of the other resistance determinants we analyzed (**Fig 4E**). These data did not provide sufficient evidence of the involvement of such mechanisms in the BRAFi tolerance of RICTOR-deficient cells.

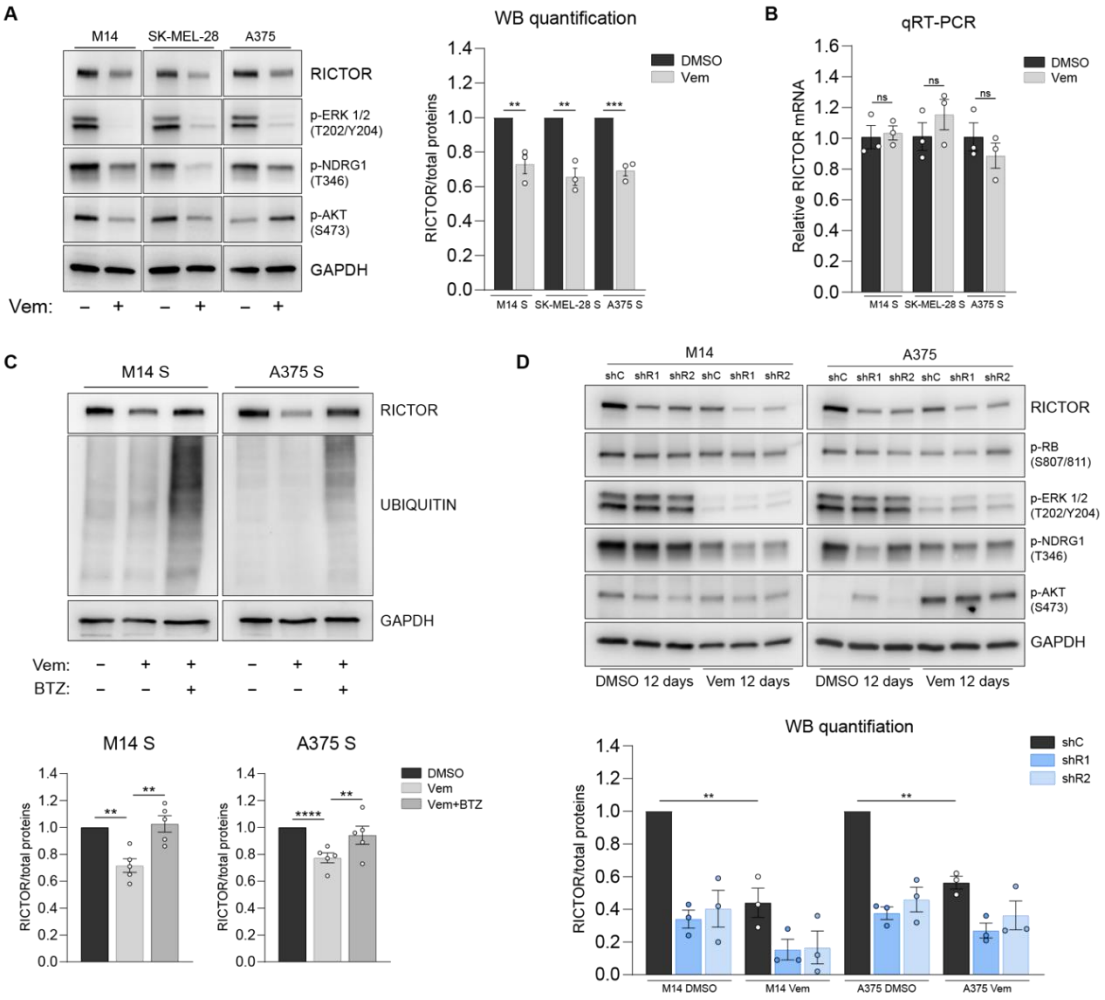

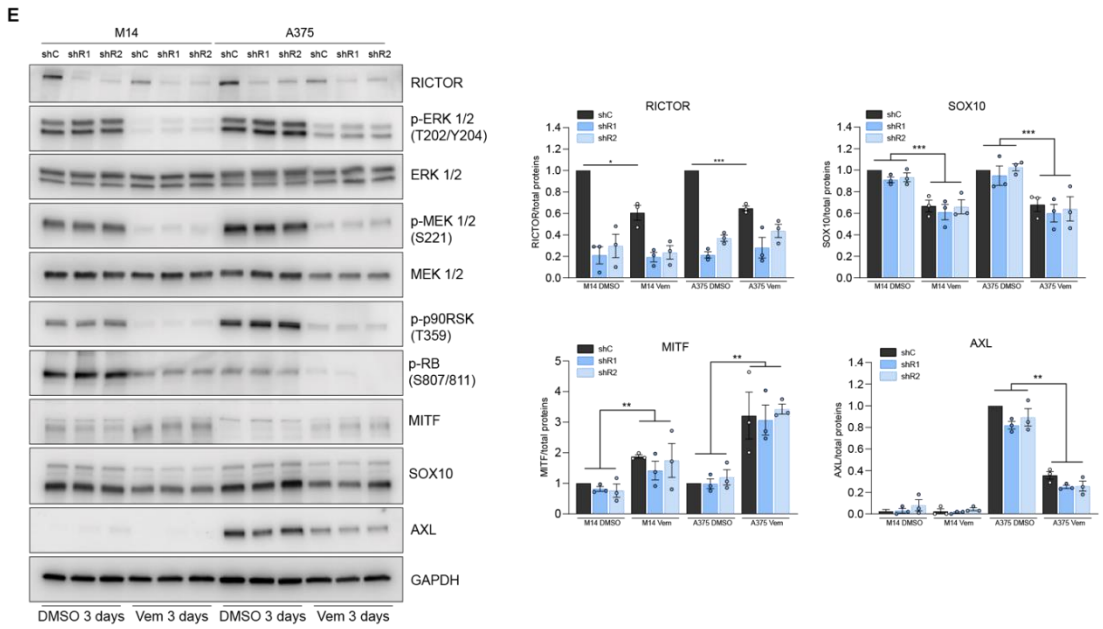

Figure 4 - RICTOR protein downregulation occurs in drug-naïve BRAFV600E melanoma cells as a consequence of MAPK pathway inhibition. A) Western blot analysis of indicated cell lines treated with (-) DMSO or (+) with 1.6 μM Vemurafenib (Vem) for 72 hours. Images are representative of 3 independent experiments. See *right panel* for quantification. **B**) qRT-PCR analysis of RICTOR gene expression in the indicated cell lines treated for 72 hours either with DMSO or 1.6 μM Vemurafenib (Vem). Bar graphs represent the mean values of 3 independent experiments ± SEM. ns = not significant, one-way ANOVA followed by Dunnett's multiple comparisons test. **C**) Upper panel: western blot analysis of indicated cell lines treated for 48 hours with 1.6 μM Vem ± 10 nM Bortezomib (BTZ). Lower panel: bar graphs show the mean values of densiometric analysis of RICTOR from 5 independent experiments ± SEM. *p < 0.05, **p < 0.01, one-way ANOVA followed by Dunnett's multiple comparisons test. **D**) Western blot analysis of indicated cell lines. Cells were cultured for 12 days in presence of either DMSO or 0.5 μM Vem. **E**) Western blot analysis of Vemurafenib-sensitive (S) and -resistant (BiR) $BRAF^{V600E}$ melanoma cell lines treated for 72 hours with (-) DMSO vehicle or (+) with 1.6 μM Vemurafenib (Vem). *Right panel* represents the quantification of indicated western blot bands intensity, each value was normalized on DMSO treated sensitive (S) cells of the same lineage. Bar graphs represent the mean values of 3 independent experiments ± SEM. *p < 0.05, **p < 0.01, ***p < 0.001, ****p < 0.0001, two-way ANOVA followed by Sidak's multiple comparisons test.

2.4 Downregulation of RICTOR in BRAFi-resistant cells has context-dependent effects

To understand the role of RICTOR in later stages of BRAFi-resistance acquisition we applied the same methodology shown in **Fig 2B** to derive BRAFi-resistant (BiR) cells from parental, drug-naïve cell lines (S). BiR cells present features of acquired resistance, such as maintenance of the resistant phenotype after drug withdrawal (**Fig 5A**) and reduced inhibition of ERK and RB phosphorylation upon Vemurafenib exposure, as compared to S counterparts (**Fig 5B**). Moreover, BiR cells also showed a lineage-specific pattern of AKT phosphorylation under basal and treated conditions while in all BiR lineages RICTOR and p-NDRG levels were no longer reduced by Vemurafenib exposure (**Fig 5B**). Consistently, also mRNA levels of RICTOR were not affected by Vemurafenib treatment (**Fig 5C**). Overall, these data indicate that RICTOR expression is positively regulated by MAPK signaling both in sensitive and resistant cells.

We then attempted to define the effects of RICTOR knockdown after the acquisition of BRAFi resistance. In all three BiR lineages, shRNA-mediated RICTOR silencing significantly impaired mTORC2 downstream signaling and the clonogenic growth of cells (**Fig 5D,E**). However, in M14

and SK-MEL-28 lineages, RICTOR knockdown led to a relative increase in clonogenic growth after treatment with BRAFi, MEKi and their combination, compared to untreated conditions (**Fig 5E *top and middle panel***). Conversely, A375 RICTOR-deficient BiR cells displayed an overall reduction in the resistance to all treatments (**Fig 5E *bottom panel***).

This underscores a context-dependent role of RICTOR after development of acquired resistance, while RICTOR knockdown in drug-naïve cells consistently promotes a faster progression towards resistance in our cellular models.

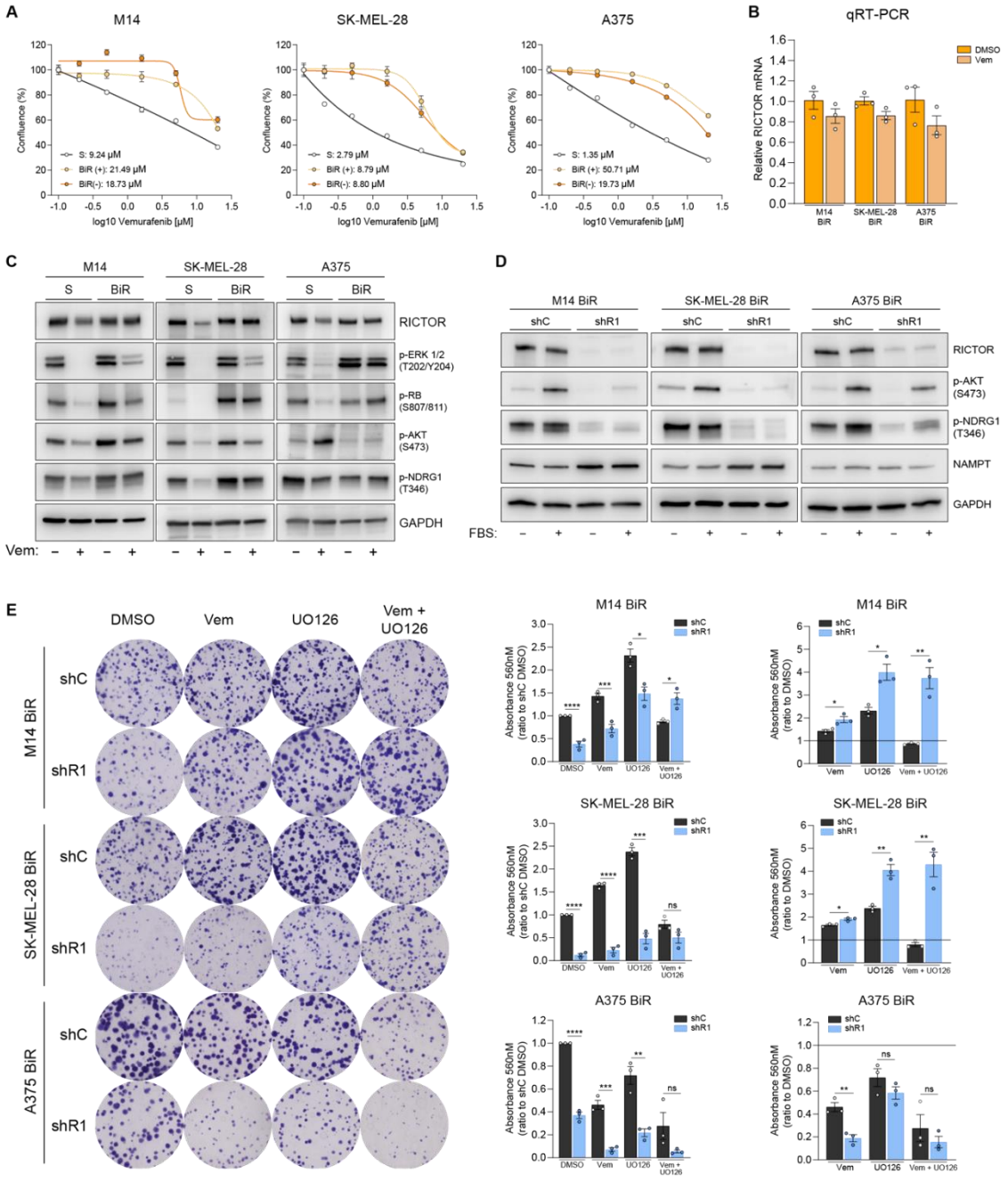

Figure 5 - RICTOR knockdown in cells irreversibly resistant to BRAFi has context-dependent effects on the response to BRAF/MEKi. A) Dose-response curves of indicated cell lines, obtained by Incucyte analysis after 72 hours of treatment with indicated doses of Vemurafenib. BiR (-) cells were cultured in the absence of Vemurafenib for 3 weeks prior to treatment while BiR (+) cells were maintained with 1.6 μM Vemurafenib; S = Vemurafenib-sensitive cells. IC50

values are displayed within each panel. **B**) qRT-PCR analysis of RICTOR gene expression performed on M14, A375 and SK-MEL-28 BiR cell lines treated for 72 hours with 1.6 µM Vemurafenib (Vem) or vehicle control (DMSO). Bar graphs represent mean values of 3 independent experiments ± SEM. ns = not significant, unpaired t-test. **C**) WB analysis of indicated cell lines treated for 72 hours with (-) DMSO vehicle or (+) with 1.6 µM Vem. **D**) WB analysis of indicated BiR cell lines transduced with scramble shRNA (shC) or with a RICTOR-targeting shRNA (shR1). Cells were analyzed after 24 hours of serum starvation (-) or 24 hours of serum starvation followed by 15 minutes of refeeding (+). Cells were kept in presence of 1.6 µM Vemurafenib. **E**) CFE assay of indicated cell lines cultured for 12 days in presence of DMSO, 1.6 µM Vem, 1 µM UO126 or the combination of 1.6 µM Vem + 1 µM UO126. Bar graphs represent the mean values of 3 independent experiments ± SEM. ns = not significant, *$p < 0.05$, **$p < 0.01$, ***$p < 0.001$, ****$p < 0.0001$, unpaired t-test. Values were normalized on untreated shC cells for each cell lineage (*middle panel*) or for the untreated condition (DMSO) of each genotype (*right panel*).

2.5 RICTOR downregulation causes PTMs changes in proteins regulating mitochondrial metabolism

To identify mTORC2-regulated molecules potentially implicated in the response of drug-naïve melanoma cells to targeted therapy, we have undertaken an unbiased proteomic approach to compare differentially expressed proteins between RICTOR-proficient and -deficient M14 and A375 cells under basal conditions. To this aim, protein extracts were separated by 2D-Gel Electrophoresis and spots were visualized by silver staining. Differentially expressed protein species were then identified by MALDI Mass Spectrometry (MS) and proteins contained in different spots displaying a fold change equal or higher than 1.5 are shown in **Table 1** and **Table 2**.

Table 1 - Differentially abundant proteins identified in RICTOR-deficient M14 cells by proteomic analysis. Column indicate protein names of the identified spots by MALDI-ToF MS, corresponding UniProt gene names, fold change expressed as the ratio between M14 shR1 and shC (means of the Volumes of single spots/Volume of total spots quantified by densitometric analysis), and the p-value determined by one-way ANOVA Test ($n = 5$)

Spot n°	Protein name	Gene name	Fold change (shR/shC)	p-value
1	Syntenin-1	SDCBP	1,64	0,0010
2	3-hydroxyacyl-CoA dehydrogenase type-2	HSD17B10	1,97	0,0011
3	Nicotinamide phosphoribosyltransferase	NAMPT	1,54	0,0014
4	Peroxiredoxin-5, mitochondrial	PRDX5	1,59	0,0025
5	Nicotinamide phosphoribosyltransferase	NAMPT	1,87	0,0027
6	Glutamine amidotransferase-like class 1 domain-containing protein 3, mitochondrial	GATD3	1,55	0,0028
7	Histone H2A type 1-H	H2AC12	1,67	0,0031
8	Triosephosphate isomerase	TPI1	1,80	0,0040
9	Pyruvate dehydrogenase E1 component subunit alpha, somatic form, mitochondrial	PDHA1	2,58	0,0044
10	UBX domain-containing protein 1 C-term fragment	UBXN6	2,69	0,0049
11	Transgelin-2	TAGLN2	1,83	0,0052
12	High mobility group protein B1	HMGB1	1,52	0,0070
13	Poly(rC)-binding protein 1	PCBP1	2,66	0,0072
14	Pirin	PIR	1,50	0,0097
15	Small ribosomal subunit protein eS12	RPS12	1,59	0,0104
16	Polyubiquitin-B [free Ubiquitin]	UBB	1,67	0,0104
17	Phosphoserine phosphatase	PSPH	2,77	0,0110
18	Triosephosphate isomerase	TPI1	1,77	0,0124
19	Superoxide dismutase [Mn], mitochondrial	SOD2	1,73	0,0124
20	Nicotinate phosphoribosyltransferase	NAPRT	1,56	0,0125
21	Prelamin-A/C	LMNA	-1,73	0,0132
22	F-box only protein 22	FBXO22	2,90	0,0158

23	Cofilin-1	CFL1	1,51	0,0173
24	Cold shock domain-containing protein E1	CSDE1	-1,56	0,0174
25	Aldo-keto reductase family 1 member A1	AKR1A1	1,53	0,0182
26	Annexin A11	ANXA11	2,48	0,0188
27	Sialic acid synthase	NANS	1,70	0,0204
28	Far upstream element-binding protein 1	FUBP1	-2,81	0,0216
29	Translation initiation factor eIF-2B subunit alpha	EIF2B1	1,54	0,0243
30	Proteasome subunit alpha type-2	PSMA2	1,58	0,0250
31	Endoplasmic reticulum resident protein 44	ERP44	1,60	0,0258
32	NADH-ubiquinone oxidoreductase 75 kDa subunit, mitochondrial	NDUFS1	4,17	0,0260
33	Tubulin alpha-1C chain Peptidyl-prolyl cis-trans isomerase FKBP4	TUBA1C FKBP4	1,51	0,0272
34	CCHC-type zinc finger nucleic acid binding protein	CNBP	2,09	0,0314
35	Scinderin	SCIN	1,54	0,0344
36	Protein S100-A4	S100A4	-3,33	0,0366
37	Alpha-centractin Elongation factor Tu, mitochondrial	ACTR1A TUFM	1,62	0,0391
38	Inosine-5'-monophosphate dehydrogenase 2 Adenylyl cyclase-associated protein 1	IMPDH2 CAP1	1,56	0,0393
39	Galectin-3	LGALS3	1,60	0,0451
40	MYG1 exonuclease	MYG1	2,31	0,0494

Table 2 - Differentially abundant proteins identified in RICTOR-deficient A375 cells by proteomic analysis. Column indicate protein names of the identified spots by MALDI-ToF MS, corresponding UniProt gene names, fold change expressed as the ratio between M14 shR1 and shC (means of the Volumes of single spots/Volume of total spots quantified by densitometric analysis), and the p-value determined by one-way ANOVA Test ($n = 5$)

Spot n°	Protein name	Gene name	Fold change (shR/shC)	p-value
1	Peptidyl-prolyl cis-trans isomerase A	PPIA	-2,29	0,0101
2	Histone H2B type 1-B	H2BC3	-2,25	0,0253
3	Hippocalcin-like protein 1	HPCAL1	-3,97	0,0342
4	GTP-binding nuclear protein Ran	RAN	2,69	0,0032
5	Eukaryotic translation initiation factor 6	EIF6	-2,84	0,0138
6	Proteasome subunit alpha type-3	PSMA3	-3,35	0,0034
7	6-phosphogluconolactonase	PGLS	-2,42	0,0062
8	Proteasome activator complex subunit 3	PSME3	-2,24	0,0217
9	Serine/arginine-rich splicing factor 1	SRSF1	-2,67	0,0120
10	Tubulin beta chain	TUBB	3,66	0,0055
11	Cathepsin Z	CTSZ	-3,50	0,0001
12	Serine-threonine kinase receptor-associated protein	STRAP	12,03	0,0215
13	Twinfilin-2	TWF2	-2,89	0,0029
14	Actin, cytoplasmic 1	ACTB	-2,63	0,0223
15	Ubiquilin-1	UBQLN1	-2,34	0,0016
16	Glycine--tRNA ligase	GARS1	-2,14	0,0370
17	Eukaryotic translation initiation factor 4B	EIF4B	-2,61	0,0062
18	Eukaryotic translation initiation factor 4B	EIF4B	-2,43	0,0008
19	Far upstream element-binding protein 2	KHSRP	3,81	0,0021
20	Elongation factor 2	EEF2	2,61	0,0222
21	Glycogen phosphorylase, brain form Elongation factor 2	PYGB EEF2	2,09	0,0336
22	Vinculin	VCL	2,14	0,0061
23	Vinculin	VCL	2,55	0,0013
24	Protein S100-A10	S100A10	-1,66	0,0106

25	Peptidyl-prolyl cis-trans isomerase A	PPIA	1,55	0,0281
26	Eukaryotic translation initiation factor 5A-1	EIF5A	-1,61	0,0022
27	Chromobox protein homolog 3	CBX3	-1,58	0,0222
28	Prohibitin 1	PHB1	-1,58	0,0094
29	Calpain small subunit 1	CAPNS1	-1,61	0,0368
30	Isopentenyl-diphosphate Delta-isomerase 1	IDI1	1,63	0,0053
31	26S proteasome non-ATPase regulatory subunit 14	PSMD14	1,46	0,0236
32	Large ribosomal subunit protein uL10	RPLP0	1,47	0,0107
33	Crk-like protein	CRKL	-1,64	0,0381
34	Elongation factor Tu, mitochondrial	TUFM	1,53	0,0332
35	Anamorsin	CIAPIN1	-1,56	0,0375
36	26S proteasome non-ATPase regulatory subunit 13	PSMD13	-1,98	0,0006
37	Leukocyte elastase inhibitor	SERPINB1	-1,80	0,0015
38	Medium-chain specific acyl-CoA dehydrogenase, mitochondrial	ACADM	1,73	0,0049
39	Elongation factor Tu, mitochondrial Isocitrate dehydrogenase [NADP] cytoplasmic	TUFM IDH1	1,56	0,0008
40	Succinate--CoA ligase [ADP-forming] subunit beta, mitochondrial	SUCLA2	1,50	0,0117
41	Ornithine aminotransferase, mitochondrial	OAT	1,63	0,0068
42	Fascin	FSCN1	-1,90	0,0422
43	S-adenosylmethionine synthase isoform type-2	MAT2A	-2,00	0,0145
44	Aldehyde dehydrogenase X, mitochondrial	ALDH1B1	1,51	0,0007
45	Ras GTPase-activating protein-binding protein 1	G3BP1	1,51	0,0009
46	Prelamin-A/C	LMNA	-1,86	0,0025
47	Sorting nexin-9	SNX9	1,70	0,0143
48	Glycogen phosphorylase, brain form Elongation factor 2 Cytoplasmic aconitate hydratase	PYGB EEF2 ACO1	1,87	0,0101
49	Nucleolin	NCL	-1,54	0,0019
50	Heterogeneous nuclear ribonucleoprotein U-like protein 2	HNRNPUL2	-1,97	0,0092
51	Talin-1	TLN1	1,65	0,0253

Gene Ontology (GO) analysis of differentially expressed protein species revealed that in both lineages, RICTOR depletion was associated with GO Cellular Components categories such as “vesicle lumen”, “ficolin rich granule lumen”, and “mitochondrial matrix” (**Fig 6A**). Among upregulated moieties, we found proteins related to oxidative stress protection (SOD2, PRDX5 [M14]), mitochondrial functions (NDUFS1, PDHA1, HSD17B10, GATD3 and TUFM [M14]; ACADM, SUCLA2, OAT, ALDH1B1 and TUFM [A375]) and NAD^+ metabolism (NAMPT, NAPRT [M14]; IDH1 [A375]). Spots identified in both M14 and A375 RICTOR-deficient cells contained TUFM, a key regulator of mitochondrial protein translation and oxidative phosphorylation(93).

Because enhanced mitochondrial respiration and increased NAD^+ biosynthesis are typical of BRAF/MEKi-resistance [PMID: 27043285, 26365896, 37779896, 23477830, 36970205] and considering that activity of some of these proteins may be regulated by post-translational modifications(94–99), we validated MS findings by 2D-Gel electrophoresis followed by Western Blot. This analysis confirmed previous results as NDUFS1, NAMPT and TUFM show different migration of specific proteoforms in RICTOR-silenced cells (representative images in **Fig 6B,C**).

Even though NAMPT and NDFUS1 spots were identified by MS as differentially expressed only in M14 cells, 2D-GE WB show changes in PTMs of both proteins also in the A375 background,

which may be due to differences in relative protein abundance of the proteins in the two cell lineages.

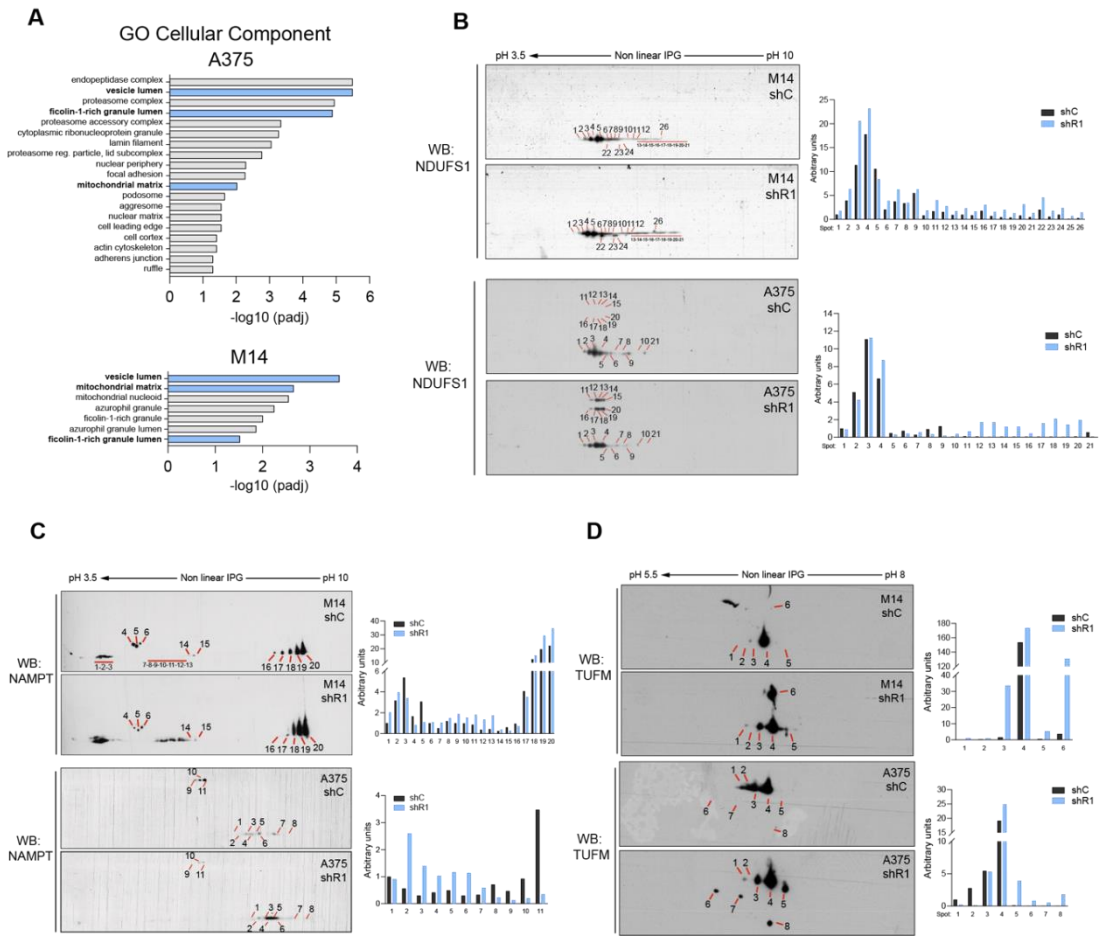

Figure 6 - RICTOR depletion in BRAF^{V600E} melanoma cells induces alterations in PTMs profiles of metabolism-regulating proteins. A) Significantly enriched gene ontology (GO) categories of differentially expressed protein species identified by MALDI-MS in shR1 M14 and A375 cells. Blue bars indicate GO terms in common between the two lineages. Redundant enriched terms relative to identical subsets of proteins have been omitted. **B-D**) Western blot analysis of NDUFS1 (**B**), TUFM (**C**) and NAMPT (**D**) proteins in the indicated cell lines performed after 2D-Gel electrophoresis (2D-GE) under basal conditions. Quantification of individual proteoforms is indicated by bar graphs on the right of each 2D-GE.

2.6 Increased mitochondrial metabolism underlies BRAFi resistance of melanoma cells

The NDUFS1 protein identified in M14 cells is the core subunit of the ETC Complex I that transfers electrons from NADH to the respiratory chain, and its overexpression enhances mitochondrial functions(100). Moreover, TUFM is a master regulator of mitochondrial translation and controls mitochondrial functions in several ways (reviewed in (101)).

Although we did not find significant changes in TUFM protein and NDUFS1 protein/mRNA levels between RICTOR-proficient and -deficient cells (**Fig 7A,B**), Seahorse analysis evidenced an overall increase in maximal respiration rates in all cellular backgrounds upon RICTOR knockdown, though some cell line-specific differences were identified for other parameters (**Fig 7C-E**). These results indicate that the increase in TUFM and NDUFS1 expression detected by MS in RICTOR-deficient cells

likely reflects the increase in proteoforms sensitive to RICTOR depletion, which may connect mTORC2 to ETC regulation. To functionally investigate the involvement of mitochondrial respiration in the BRAFi-resistant phenotype of shR cells, we carried out CFE survival assays in the presence of Vemurafenib and/or the ETC Complex I inhibitor Phenformin, a derivative of the anti-diabetic drug Metformin(102). Whereas treatment with Phenformin alone similarly reduced of ~40% the clonogenic ability of both RICTOR-deficient and –proficient cells under basal conditions, when combined with Vemurafenib it selectively diminished the CFE of RICTOR-deficient cells to levels comparable to those of BRAFi-sensitive control cells (**Fig 7F**). These data indicate that ETC complex I inhibition induces a substantial rescue of the BRAFi-tolerant phenotype of shR cells, further indicating that mitochondrial respiration plays an important role in protecting these cells from BRAF inhibition.

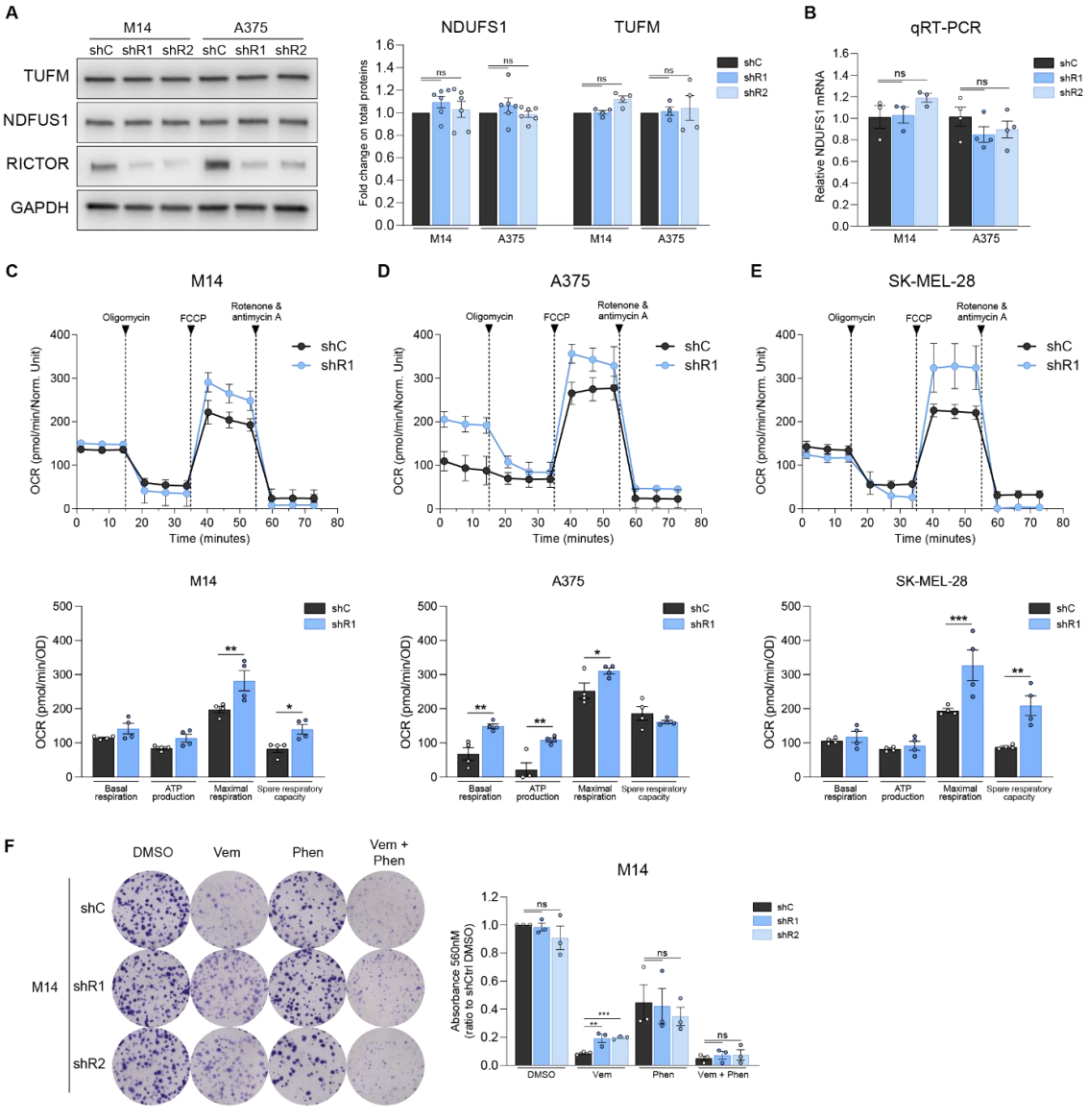

Figure 7 - Increased mitochondrial respiration underlies the BRAFi resistance of RICTOR-deficient melanoma cells. A) Western blot analysis performed on indicated cell lines under basal conditions. **B**) qRT-PCR analysis of NDUFS1 gene performed on indicated cell lines. Bar graphs represent the mean values of 4 independent experiments ± SEM. ns = not significant, one-way ANOVA followed by Dunnett's multiple comparisons test. **C-E**) OCR measurement performed on indicated cell lines using Seahorse XFp analyzer. Bar graphs under each curve represent functional parameters calculated from the same measurements (n = 4). *p < 0.05, **p < 0.01, ***p < 0.001 one-way ANOVA followed by Sidak's multiple comparisons test. **F**) CFE assay of indicated cell lines cultured for 12 days in presence of DMSO, 0.5 μM Vemurafenib (Vem), 200 μM Phenformin (Phen) or the combination of 0.5 μM Vemurafenib + 200 μM Phenformin (Vem + Phen). Bar graphs represent the mean values of 3 independent experiments ± SEM. **p < 0.01, ***p < 0.001, one-way ANOVA followed by Dunnett's multiple comparisons test.

2.7 Increased NAMPT activity is crucial for BRAFi resistance of RICTOR-depleted cells

Our proteomic analysis also identified in RICTOR-depleted M14 cells an increase in the expression of proteins involved in NAD^+ metabolism and biosynthesis (NAMPT, NAPRT, IDH1). Specifically, NAMPT is the rate-limiting enzyme of the NAD^+ salvage pathway in mammals and increases in its expression/activity play key roles in melanoma therapeutic resistance to BRAF/MEKi(53,103). Albeit M14 and A375 cell lines differ in their absolute levels of NAMPT protein expression, in both lineages, RICTOR knockdown induced a significant increase in NAMPT levels relative to control conditions (**Fig 8A**). RICTOR-depleted M14 cells also displayed increased NAMPT mRNA levels, while RICTOR-proficient and –deficient A375 cells possessed similar level of *NAMPT* transcript (**Fig 8B**). Measurements of NAMPT catalytic activity revealed an increase in M14 shR cells, both under basal conditions and upon Vemurafenib treatment (**Fig 8C**). In A375 shC cells NAMPT activity was found below the threshold of detection of our enzymatic assay (< 0.10 pmol/h/μg), which is likely due to their intrinsically lower NAMPT levels compared to the M14 cell lineage (**Fig 8A**). Nevertheless, in shR A375 cells, NAMPT activity was measurable both under basal conditions and upon Vemurafenib treatment (0.183 pmol/h/μg and 0.123 pmol/h/μg, respectively), indicating that also in this cell lineage the catalytic activity of the enzyme is increased by RICTOR depletion.

Overall, our analysis revealed that RICTOR deficiency is coupled to an increased NAMPT protein expression and/or activity in $BRAF^{V600E}$ melanoma cells, and that both transcriptional and post-transcriptional mechanisms can account for this effect in a cell lineage-specific manner.

To verify whether in shR cells the overall increase in NAMPT activity plays a role in their BRAFi resistance, we compared the survival of mTORC2-deficient and –proficient cells by CFE assays carried out in the presence of Vemurafenib and/or two structurally unrelated NAMPT inhibitors (NAMPTi), FK866 and OT-82 (**Fig 8D,E**). Similar to Phenformin treatment, exposure of cells to low nanomolar concentrations of both FK866 and OT-82 caused a comparable reduction of CFE in both genotypes. In the A375 cellular background, FK866 alone caused a more pronounced drop in cell clonogenicity in all genotypes as compared to the M14 lineage. In the latter, the combination of Vemurafenib + FK866 or OT-82 caused a drop in the clonogenicity of RICTOR–deficient cells equivalent to that observed in control cells. Thus, the inhibition of NAMPT enhances the response of RICTOR-deficient cells to Vemurafenib, indicating that the increased activity of the enzyme in these cells is critical for their BRAFi resistance.

To verify if the NAMPT-dependent BRAFi-resistant phenotype induced by RICTOR depletion holds true also *in vivo,* we injected M14 RICTOR-deficient and -proficient cells subcutaneously in NOD/SCID/IL2γr^{null} (NSG) mice, and when tumors became palpable, mice were treated with Vemurafenib and/or FK866. Tumor growth was progressively monitored, and after 14 days of treatment the animals were sacrificed, and tumors were measured and weighted. As shown in **Fig 8F,G**, whereas tumors generated by RICTOR-proficient cells displayed a decrease in weight of about 50% in response to Vemurafenib, weight and the volume of RICTOR-deficient tumors at the experimental endpoint were comparable to that of vehicle-treated. The combination of Vemurafenib and FK866 induced instead in RICTOR-deficient tumors a growth inhibition similar to that of Vemurafenib-treated control tumors. The sensitivity of RICTOR-deficient and -proficient xenografts to the treatment with NAMPTi alone differed between the two genotypes, as shR tumors resulted overall less responsive to the individual FK866 treatment. Nevertheless, even in this *in vivo* setting, NAMPT inhibition combined to Vemurafenib treatment significantly enhanced the responses of RICTOR-deficient xenografts to Vemurafenib, confirming that NAMPT activity is key for counteracting the response of these tumors to BRAFi.

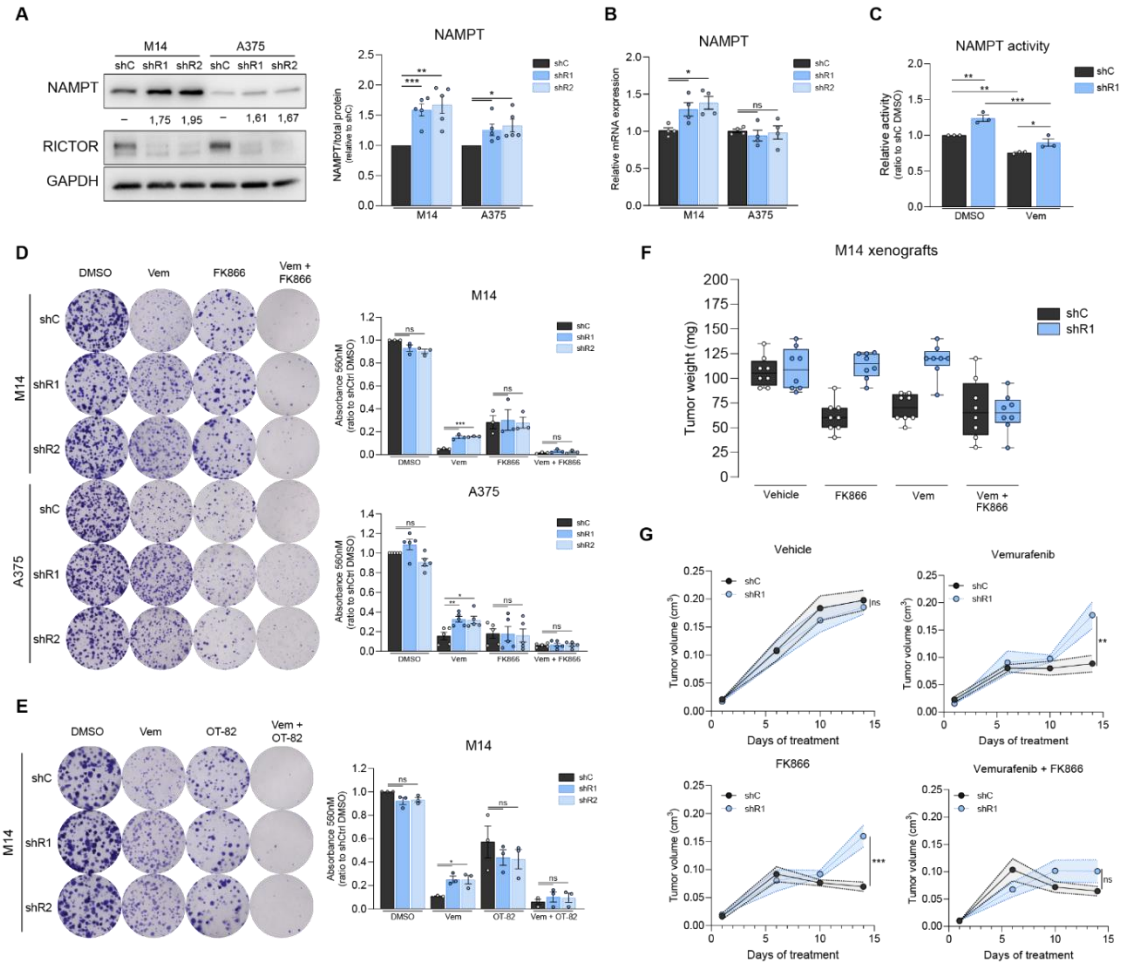

Figure 8 - Increased NAMPT activity is crucial for BRAFi resistance of RICTOR-depleted cells *in vitro* and *in vivo*. **A**) WB analysis performed on indicated cell lines under basal conditions. Densitometric quantification of NAMPT band intensity is indicated below each band. *Right panel*: densitometric quantification of WB, each value was normalized on shC cells of the same lineage. Bar graphs represent the mean values of 5 independent experiments ± SEM. *p < 0.05, **p < 0.01, ***p < 0.001, one-way ANOVA followed by Dunnett's multiple comparisons test. **B**) qRT-PCR analysis of

NAMPT gene expression in the indicated cell lines under basal conditions. Bar graphs represent mean values of 4 independent experiments ± SEM. *p < 0.05, one-way ANOVA followed by Dunnett's multiple comparisons test. **C**) NAMPT enzymatic activity of M14 cells treated for 24 hours with 5 μM Vemurafenib (Vem) or vehicle control (DMSO), normalized on untreated shC cells. Bar graphs represent mean values of 3 independent experiments ± SEM. *p < 0.05, **p < 0.01, ***p < 0.001, two-way ANOVA followed by Tukey's multiple comparisons test. **D**) CFE assay of indicated cell lines cultured for 12 days in presence of DMSO, 0.5 μM Vem, 2.5 nM FK866 or the combination of 0.5 μM Vem + 2.5 nM). Bar graphs represent the mean values of independent experiments ± SEM (n = 3 for M14 cells; n = 4 for A375 cells). *p < 0.05, **p < 0.01, ***p < 0.001, ****p < 0.0001, one-way ANOVA followed by Dunnett's multiple comparisons test. **E**) CFE assay of M14 cells cultured for 12 days in presence of DMSO, 0.5 μM Vem, 1.2 nM OT-82 or the combination of 0.5 μM Vem + 1.2 nM OT). Bar graphs represent the mean values of 3 independent experiments ± SEM. *p < 0.05, one-way ANOVA followed by Dunnett's multiple comparisons test. **F**) Tumor weights of tumor xenografts of shC or shR1 M14 cells in NSG mice (n = 8 mice/group), treated for 14 days with the indicated drugs. **p < 0.01, ***p < 0.001, ****p < 0.0001, two-way ANOVA followed by Tukey's multiple comparisons test. **G**) Growth curves of M14 shC or shR1 xenografts used for tumor weight measurement, each graph refers to the treatment indicated at the top. *p < 0.05, **p < 0.01, two-way ANOVA followed by Tukey's multiple comparisons test performed at the experimental endpoint.

3. DISCUSSION

Our research uncovers an unforeseen role for RICTOR/mTORC2 downregulation in promoting the development of resistance to BRAFi-based therapies in $BRAF^{V600E}$ melanoma cells. This discovery seems at odds with the well-established role of mTORC2 signalling in promoting cell growth and survival across various pathophysiological contexts(104–107), including melanoma progression(106,107). However, our findings align with emerging evidence indicating tumor suppressive functions for mTORC2 in different settings(77,108,109).

In fact, we show that RICTOR silencing in drug-naïve cells accelerates the acquisition of resistance to Vemurafenib, indicating a role for mTORC2 downregulation during the early adaptation to BRAFi. This was demonstrated with a resistance-acquisition assay, in which sensitive cells (both RICTOR-silenced and controls) are cultured with increasing doses of BRAFi until they develop features of acquired resistance (i.e. stable proliferation in presence of the drug, unreversible resistance). By keeping track of the days required for each cell line to develop resistance to relatively high dose of Vemurafenib, we found that RICTOR-silenced variants reach the experimental endpoint several days/weeks earlier than their controls. A similar phenomenon could also take place in melanoma patients with lower intratumoral levels of RICTOR and thus negatively affect their response to targeted therapy. Interestingly, RICTOR-silenced variants which display stronger reduction of RICTOR protein within a cell line also reach full resistance earlier (more evident by comparison between A375 shR1 and A375 shR2). Faster development of resistance in the first phases may be linked to a reduced initial response, which primes the cells to shift towards “stronger” resistance more rapidly.

Indeed, clonogenic assays showed that RICTOR-depleted cells exhibit intrinsic tolerance to BRAFi, either alone or in combination with MEKi. The adaptive role of RICTOR downregulation in the resistance development is further supported by the observation of endogenous RICTOR decline during the initial phase of response of drug-naïve cells to BRAF inhibition. Of note, we described this decrease also in cellular colonies surviving sustained Vemurafenib treatment, which likely represent the precursors of future BRAFi-resistant cell populations. Thus, RICTOR downregulation may regulate adaptation and development of resistance to BRAFi in different steps.

Our data suggest that a decrease in MAPK signaling is the primary trigger for this phenomenon, which occurs through processes leading to the reduction of RICTOR protein levels. Although the specific molecular mechanism remains unidentified, we propose that BRAFi-induced RICTOR downregulation relies on the modulation of its protein stability, as it is sensitive to proteasomal inhibition and unrelated to changes in mRNA levels. Likewise, BiR variants display a much smaller degree of MAPK pathway inhibition after Vemurafenib treatment and do not downregulate RICTOR protein, supporting the hypothesis that RICTOR levels are regulated downstream of BRAF.

Interestingly, BiR variants display similar levels of RICTOR protein compared to their sensitive counterparts, suggesting that reduction of RICTOR protein may be a transitory phenomenon that characterizes the first phases of TT-resistance acquisition and is dispensable in the later phases.

These data are consistent with recent findings that highlight the importance of post-translational mechanisms on the overall regulation of RICTOR/mTORC2 in different models(110–113). However, it remains possible that other unidentified factors (like microRNAs or changes in mRNA translation) may also contribute to regulate RICTOR protein at different stages of melanoma progression(112,114–116). Specifically, the E3 ubiquitin ligase FBXW7 (F-box and WD repeat domain-containing 7) has been shown to be regulated by ERK in some cancers, to control RICTOR levels and to promote melanoma progression/therapeutic resistance(111,117–119).

Preliminary data shows that in our context FBXW7 protein levels are not directly affected by BRAFi treatment, but we could not completely exclude that in these conditions BRAFi regulate RICTOR protein by affecting its interaction with FBXW7.

In many cases, mTORC2 functions have been approached as a prospective target in tumor cells displaying advanced stages of therapeutic resistance. These cells are also typically characterized by upregulation in growth factor receptor signaling(17), for which mTORC2 acts as amplifier of mitogenic stimuli(68). Consistently, we found a generalized decrease in basal clonogenicity after inducing RICTOR depletion in irreversibly resistant cells. However, our study shows that the specific response of RICTOR-deficient BiR cells to BRAF/MEKi in this context ranges from an increased sensitivity (in A375 BiR cells) to a stimulation of clonogenicity to BRAF/MEKi (in M14 and SK-MEL-28 cells). The described behaviour of BiR A375 cells is in agreement with the finding of Jebali et al.(107), that showed enhanced responses of BRAFi-resistant A375 cells to mTOR(C2) inhibition.

Thus, although the effects of RICTOR depletion in the responses of cells to targeted therapy may vary in BiR cells, RICTOR knockdown in drug-naïve cells consistently promotes a faster progression towards BRAFi resistance.

Proteomic analysis of RICTOR-deficient cells revealed significant alterations in proteins related to NAD^+ biosynthesis and mitochondrial processes. We observed that RICTOR knockdown correlates with increased NAMPT expression/activity, with multi-layered and cell lineage-specific mechanisms leading to NAMPT upregulation. RICTOR deficiency alters post-translational modifications in NAMPT likely affecting its activation and/or stability, which is suggestive of a complex interplay between mTORC2 signaling and NAD^+ biosynthesis in melanoma. 2D proteomic analysis also identified a differential representation of NDUFS1 and TUFM proteoforms, suggesting mTORC2 regulation on mitochondrial dynamics in melanoma. This is further supported by GSEA analysis of melanoma TCGA data, which indicates upregulation of mitochondrial gene signatures in low RICTOR tumors. The connection between increase in mitochondrial functions and resistance to BRAFi is supported by our experimental evidence, as both NAMPT and ETC inhibition reverses the BRAFi tolerance of RICTOR-depleted cells. Our

findings are supported by previous works that show NDUFS1 modulation by post-translational modifications, and by poorly-characterized associations between RICTOR downregulation and gain of mitochondrial functions(94,120,121).

The clinical significance of our findings is supported by analysis of the cutaneous melanoma subset in the TCGA database, which reveals a positive correlation between lower RICTOR protein and poorer outcomes in patients with $BRAF^{V600E}$ mutations. Conversely, higher levels of RAPTOR mRNA correlate with worse prognosis, consistent with the pro-tumorigenic role of mTORC1 in melanoma(76). These results suggest that the use of pan-mTOR inhibitors, often proposed in the context of melanoma treatment(105,122), could potentially represent a double-edged sword, with mTORC1 inhibition potentially counteracting therapeutic resistance while mTORC2 inhibition may exacerbate it.

This highlights the importance of assessing RICTOR protein levels for diagnostic and prognostic purposes, given the poor correlation between RICTOR mRNA and protein levels in melanoma patients.

Accordingly, patients with low RICTOR tumors may benefit from NAMPTi therapy in combination with targeted therapy, with low RICTOR levels serving as a predictive biomarker for NAMPTi response, thus improving the applications of NAMPT inhibitors in the clinics.

An outstanding question is whether Immune Checkpoint Inhibitors would represent a valuable alternative for the treatment of BRAF-mutated low RICTOR tumors. This is especially relevant in light of recent evidence that connect tumor immunogenicity with metabolic alterations reminiscent of those we observed in RICTOR-deficient cells(123,124).

In conclusion, our study reveals an important role for RICTOR/mTORC2 in modulating response to BRAFi therapy, highlighting potential therapeutic avenues. In particular, RICTOR protein may serve as a suitable biomarker for guiding therapeutic strategies, rather than as an actionable target *per se*, as often proposed. These findings strongly emphasize the need for personalized treatment strategies based on tumor molecular profiles.

4. MATERIALS AND METHODS

Cell culture

A375, M14 (MDA-MB-435S) and SK-MEL-28 cells were obtained from the American Type Culture Collection (ATCC) and maintained in Dulbecco's modified Eagle's medium (DMEM, Gibco 10566016) supplemented with 10% (v/v) fetal bovine serum (FBS, Gibco 10270106), 1% MEM Vitamin Solution (Gibco, 11120037), 1% MEM Non-Essential Amino Acids Solution (Gibco, 11140035), 10mM HEPES Buffer Solution (Gibco, 15630056) and 1% Penicillin-Streptomycin (Gibco, 15140122). Cells were maintained in these culture conditions for all experiments except where specifically indicated. All cell lines were authenticated by PCR-single-locus-technology by Eurofins Genomics (Ebersberg, DE) and were routinely tested for Mycoplasma contamination.

Colony Forming Efficiency (CFE) assay

Cells were seeded at 500 cells/well in 6-well plates and treated with the indicated drugs the following day. Media with the drugs was refreshed every 72 hours and cells were cultured for 12 days. At the endpoint cells were fixed with 4% paraformaldehyde for 15 minutes, rinsed with PBS and stained with 0.1% crystal violet. Staining intensity was quantified by dissolving crystal violet with 1 ml of 10% acetic acid for 15 minutes, then 100 µl were moved in 96-well plate and optical density (OD) was measured by 560nm absorbance using Promega GloMax Explorer GM3500.

For Colony Forming assay of siRNA-transfected cells, cells were seeded at 2000 cells/plate 24 hours after transfection and treated with the indicated drugs the following day. Media with the drugs was refreshed every 72 hours and cells were cultured for 7 days. Staining and intensity quantification were performed as described above.

BRAFi resistance acquisition assay

Parental BRAFi-sensitive cells were seeded in 60 mm cell culture dishes (1.5 x 10^5 cells/dish) and after 24 hours treated with 0.2 µM Vemurafenib, then maintained in the presence of the same drug concentration with media refresh every 72 hours. When cells reached confluency, they were collected and re-plated in new 60mm dishes (1.5 x 10^5 cells/dish). Cells were then treated with a higher dose of Vemurafenib and the same process was repeated when they reached confluency in the presence of the new Vemurafenib dose. Vemurafenib doses used for this experiment are indicated in **Fig. 2B** (0.2 - 0.4 - 0.8 - 1.2 - 1.6 µM) and cells were considered fully resistant when they could grow in the presence of 1.6 µM Vemurafenib.

In vivo experiments

6-8 weeks-old NOD scid gamma (NSG) mice were purchased by Charles River Laboratories International (Wilmington, MA, USA) and were maintained in a specific-pathogen-free (SPF) facility of the Molecular Biotechnology Center (MBC, UniTo, Italy). 5 x 10^6 M14 cells were resuspended in Matrigel® (Corning) and subcutaneously injected in the flank of mice, when tumors became palpable mice were treated as follows: FK866 was administered intraperitoneally

(50µl/twice daily/14 days at 20 mg/kg), while BRAFi was administered by gavage (200µl/daily/14 days at 60 mg/kg). The vehicle condition was treated in the same way administering a solution without the drug. The tumor size was measured weekly using calipers in two dimensions to generate a tumor volume using the following formula: 0.5 × (length × width^2). After 14 days from the start of the treatment mice were euthanized and tumors were collected and weighed. Procedures were conducted in conformity with national and international laws and policies as approved by the Faculty Ethical Committee and the Italian Ministry of Health.

RICTOR downregulation with shRNA and siRNA

Stable RICTOR-silenced cell lines were generated by lentiviral transduction of two independent RICTOR-targeting shRNAs (Addgene #1853 and #1854), while control shC cells were generated by lentiviral transduction of scramble shRNA (Addgene #1864) of the same cells of origin. Target cells (M14, A375, SK-MEL-28) were incubated with lentiviral vector-containing supernatant supplemented with Sequa-brene (Sigma-Aldrich) at a final concentration of 8 µg/mL. After 20 hours incubation, lentiviral vector-containing supernatant was substituted with fresh growth medium, and the following day selection antibiotic was added (Puromycin, 2 µg/ml). Transduced cells were expanded under continuous antibiotic selection, and all experimental procedures were carried out in the absence of Puromycin.

Transfection of RICTOR targeting (#L-016984-00, Horizon Discovery, Cambridge, UK) or non-targeting pool (#D-001810-10, Horizon Discovery) was performed using Lipofectamine 3000 (Invitrogen) according to manufacturer's instructions. Briefly, 250000 cells were seeded in 60 mm dishes at day 1 and after 24 hours were transfected using Lipofectamine 3000 reagent and 0,7 µmoles of each siRNA. 24 hours post-transfection cells were trypsinized and plated in 6-well plates (2000 cells/well) for Colony Forming Efficiency, or for Western Blot analysis.

Western blotting

Cells seeded on culture plates were frozen in liquid nitrogen before lysis. Cells were scraped on ice with cold lysis buffer (1% Triton X-100, 50 mM Tris/HCl pH 7.4, 150 mM NaCl, 1mM EDTA) supplemented with 1 mM PMSF, 1 mM Na_3VO_4, 10 mM NaF, 1X cOmplete Protease Inhibitors Cocktail (Roche, Basel, Switzerland) and 10 mM sodium butyrate. Lysates were centrifuged at 14000g for 15min at 4°C and protein concentration was measured using the Bradford assay (Bio-Rad, Hercules, CA, USA). Lysates were diluted in Laemmli buffer and boiled for 10 minutes at 95°C. Equal amounts of proteins were loaded on 4–15% Mini- PROTEAN® TGX™ Precast Protein Gels (Bio-Rad) and transferred to PVDF Transfer Membrane (Merck Millipore, Billerica, MA, USA). Membranes were blocked in 5% non-fat dry milk (Santa Cruz Biotechnology, Dallas, TX, USA) in Tris-buffer saline, 0.1% Tween20 and incubated with the indicated antibodies following the manufacturer's instructions.

The following antibodies were used: Rictor (#9476), Sin1 (#12860), Phospho-Akt (Ser473) (#4060), Phospho-NDRG1 (Thr346) (#5482), Phospho-p44/42 MAPK (Erk1/2) (Thr202/Tyr204) (#4370), p44/42 MAPK (Erk1/2) (#4695), Phospho-MEK1/2 (Ser221) (#2338), MEK1/2 (#9122),

Phospho-p90RSK (Thr359/Ser363) (#9344), NDUFS1 (#70264), PBEF/NAMPT (#61122), Phospho-RB (S807/811) (#8516), SOX10 (#D5V9L), AXL (#8861), Ubiquitin (#3936) from Cell Signaling Technology (Danvers, MA, USA); GAPDH (AM4300) from Invitrogen (Waltham, MA, USA); TUFM (#MA5-31364) from Thermo Fisher (Waltham, MA, USA); MITF (#NBP1-88618) from Novus Biologicals (Centennial, CO, USA); Horseradish peroxidase-conjugated secondary antibodies from Sigma-Aldrich. Immunoblots were developed by chemiluminescence with ECL (Clarity Western ECL Substrate, Bio-Rad), acquired with the molecular imager ChemiDoc XRS, and quantified by densitometric analysis using the Image-lab software (Bio-Rad). All comparative images of immunoblots were obtained by exposure of the same membranes.

Seahorse Metabolic Experiments

Real-time measurements of oxygen consumption rate (OCR) were made using an XF Extracellular Flux Analyzer (Agilent Technologies, Santa Clara, CA). Cells were seeded in XFe96 plates (Agilent) at 30000 cells/well and OCR was measured using the XFe96 Extracellular Flux Analyzer and the XF Cell Mito stress test kit (Agilent) according to the manufacturer's instructions. Cells in XF Mito stress media (DMEM supplemented with 10 mM glucose, 2 mM glutamine and 1 mM pyruvate, pH 7.4) were incubated at 37 °C in the absence of CO_2 for 1 h. Baseline OCR measurements were determined before administration of oligomycin (1 mM), FCCP (1 mM), and a combination of rotenone and antimycin A (0.5 mM). OCR data were obtained and analyzed using the XF Cell Mito Stress Test Generator software (Agilent Seahorse Bioscience).

Lentiviral vector Production

Lentiviral vectors were generated as described in (125). Briefly, 3 x 10^6 HEK-293T cells were plated in a 10 cm cell culture dish in DMEM media supplemented with 10% FBS without penicillin/streptomycin. 24 hours post-plating, cells were incubated overnight with transfection reaction consisting of Lipofectamine 2000 (Invitrogen) and DNA plasmids, both diluted in Opti-MEM (Thermo-Fisher Scientific) following the manufacturer's instructions. The following plasmids were used: pMD2-VSV-G (envelope plasmid), pCMV-dR8.74 (packaging plasmid) and transfer plasmid (pLKO.1-scramble/Rictor_1/Rictor_2 shRNA). After overnight incubation, the supernatant was removed and replaced with fresh medium. Lentivirus-containing supernatant was collected after 48 hours, filtrated (0.22 µm pore), aliquoted and stored at -80°C until use.

Reagents

Vemurafenib, UO126, FK866 used for *in vitro* experiments were purchased from Selleckchem (Houston, TX, USA), OT-82 was purchased from Selleckchem, Bortezomib was purchased from Sigma-Aldrich (St. Louis, MO, USA). Vemurafenib and FK866 used for *in vivo* experiments were purchased from MedChem Express (Monmouth Junction, NJ, USA). Phenformin hydrochloride was purchased from Sigma-Aldrich (St. Louis, MO, USA).

For *in vivo* experiments, FK866 was diluted in an aqueous solution containing 30% propylene glycol, 5% Tween-80 and 5% dextrose (all reagents from Sigma) at a concentration of 10 mg/Kg,

while Vemurafenib was diluted in an aqueous solution containing 21% DMSO, 30% PEG-400, 0.5% Tween-80 and 5% propylene glycol (all reagents from Sigma) at a concentration of 30 mg/Kg.

Determination of drug sensitivity

Cells were seeded into 96-well plates (2500 cells/well) and treated with the indicated drug doses of Vemurafenib the following day. The plates were placed in an IncuCyte SX5 Live-Cell Analysis System (Essen BioScience, Ann Arbor, Michigan, USA) for 72 hours, with images acquired every 4 hours. Cell confluence was measured and quantified by the IncuCyte imaging system (Essen Bioscience). IC50 values were calculated at the endpoint using the online tool Quest Graph™ IC50 Calculator (AAT Bioquest, Inc., Sunnyvale, CA, USA).

Growth assay

Cells were seeded (M14 40000 cells/well; A375 30000 cells/well) into 12-well plates (one plate for each time point) and media change was performed the following day. 24, 48, 74 and 96 hours after media change, cells were fixed with 4% paraformaldehyde for 15 minutes, rinsed with PBS and stained with 0.1% crystal violet. Staining intensity was quantified by dissolving crystal violet with 250 µl of 10% acetic acid for 15 minutes, then 100 µl were moved in 96-well plates and optical density (OD) was measured by 560nm absorbance using Promega GloMax Explorer GM3500.

NAMPT activity measurement

The assay allows determination of NAMPT activity by converting NMN to NAD^+, via three consecutive reactions consisting of NMN deamidation to NaMN, NaMN adenylyation to NaAD, and NaAD conversion to NAD^+. The reactions are catalyzed by the bacterial recombinant enzymes NMN deamidase (PncC), NaMN adenylyltransferase (NadD) and NAD synthetase (NadE). The formed NAD^+ is finally quantitated by a fluorometric cycling assay(126).

Briefly, cells ($2x10^7$) were washed twice with PBS, and cell pellets were resuspended in 200 µl of 50 mM TRIS/HCl, pH 7.5, 0.15 M NaCl, 1 mM DTT, 1 mM PMSF, 0.002 mg/ml leupeptin, antipain, chymostatin and pepstatin. The suspension was sonicated three times for 1 min at 50 W, with 1 min intervals, and centrifuged at 7000 rpm for 15 min at 4°C. The supernatants were immediately used, and the protein concentration was measured using the Bradford assay (Bio-Rad, Hercules, CA, USA).

The assay mixture contained ethanol buffer (30 mM HEPES, pH 8.0, 1 % v/v ethanol, 8.4 mg/ml semicarbazide), 40 mM HEPES/KOH, pH 7.5, 10 mM KF, 10 mM $MgCl_2$, 2.5 mM ATP, 0.05 mM Nam, 1.0 mM PRPP, 6 Units/ml ADH (Sigma A3263), 0.067 mg/ml BSA, 1 Units /ml NadD, 0.03 Units /ml PncC, and 0.25 mg/mL of cell extracts, in a final volume of 135 µL. A control mixture in the presence of 5 µM FK866 was also processed in parallel. Reaction mixtures were incubated at 37°C, and at suitable time intervals, 30 µl aliquots were withdrawn and added with half their volume of 1.2 M cold $HClO_4$ to stop the reaction. After 15 minutes on ice, samples were

centrifuged (20000 g, 5 minutes), and supernatants were neutralized with 1 M K_2CO_3. After centrifugation, 40 µl aliquots were transferred into a flat-bottom 96-well black plate. NaAD conversion to NAD^+ was started by adding 50 mM HEPES, pH 7.5, 0.15 M KCl, 1.4 mM ATP, 50 mM NH_4Cl, 11 mM $MgCl_2$ and 0.06 U/ml NadE, to a final volume of 145 µl. After incubation (30 minutes, 37 °C) the NAD^+ cycling reaction was started by adding 96 µl of cycling reagent to each well. The cycling reagent, freshly prepared, contained 100 mM sodium phosphate, pH 8.0, 2% ethanol, 32 µM resazurin, 10 U/mL ADH, 0.1 mg/mL BSA, 10 µM flavin mononucleotide and 0.1 mg/mL diaphorase that was previously purified through a PD MiniTrap Sephadex G-25 column (GE Healthcare) equilibrated and eluted with 10 mM sodium phosphate buffer, pH 8.0. Following addition of the cyclic reagent, the resorufin fluorescence was measured continuously in each well using a Synergy HT microplate reader (Bio-Tek, Winooski,VT, USA) equipped with 544 and 590 nm excitation and emission filters, respectively. The amount of NaAD present in the wells, corresponding to the amount of NMN formed by the enzyme, was calculated by interpolating on a NaAD standard curve the corresponding rate of fluorescence increase, after subtracting the respective control. The results were expressed as pmoles of product formed /hour/µg protein and are means ± standard deviation of two independent experiments. The ancillary bacterial enzymes PncC, NadD, and NadE were prepared as described(126).

NAD^+ level measurement

Pellets from about $3x10^5$ cells were resuspended in 0.15 mL of 0.4 M cold $HClO_4$. After centrifugation at 2300 g for 10 min at 4°C, the supernatants were neutralized with 1.0 M K_2CO_3. Neutralized samples were then centrifuged as described above and pellets were resuspended in 0.1 mL formic acid for protein determination using the Bradford assay. NAD^+ was measured in the supernatants through the fluorometric cycling assay described in the previous section, by adding a suitable amount of sample diluted in 0.145 mL of water to 96 µl of cycling reagent. The increase in resorufin fluorescence was measured as described. The amount of NAD^+ was calculated by interpolation on a NAD^+ standard curve and the results were expressed as nmol NAD^+/mg protein. Data are means ± standard deviation of two independent experiments.

RNA isolation and qRT-PCR

RNA was isolated from cells using TRIzol reagent (Invitrogen) according to the manufacturer's instructions and converted to cDNA using the High Capacity cDNA Reverse Transcription kit (Thermo Fisher Scientific). qRT-PCR was performed using the 7900 HT Fast Real Time PCR system (SDS2.3 software) using commercially available primers (TaqMan Gene Expression Assays; Thermo Fisher Scientific): Hs00237184_m1 (*NAMPT*), Hs00192297_m1 (*NDUFS1*), Hs00380903_m1 (RICTOR), Hs99999903_m1 (*ACTB*, used ad housekeeping gene). Comparative CT methods was used to calculate the relative expression of the gene under analysis.

2D Gel electrophoresis

2D-Electrophoresis (2DE) was performed using the Immobiline polyacrylamide system(127). Immobilized nonlinear pH 3-10 gradient on strips 18 cm in length (Cytiva, Uppsala, Sweden) (formerly GE Healthcare) were employed in the first dimensional run carried out by Ettan™ IPGphor™ Manifold (GE Healthcare, Uppsala, Sweden) at 16 °C with the following electrical conditions: 200 V for 8 h, from 200 V to 3500 V in 2 h, 3500 V for 2 h, from 3500 V to 5000 V in 2 h, 5000 V for 3 h, from 5000 V to 8000 V in 1 h, 8000 V for 3 h, from 8000 V to 10000 V in 1 h, 10000 V for 10 h for a total of 90,000 VhT. Mass Spectrometry (MS)-preparative strips were pre-rehydrated overnight with 350 µl of denaturing solution. Samples added with 0.2% of carrier ampholytes for the analytical runs and 2% for the preparative ones, were loaded by rehydration loading and cup at the cathodic ends of the IPGstrips, respectively. At the end of the first dimensional run, strips were washed with deionized water and equilibrated with two buffers: the first composed of 6 M Urea, 2% w/v Sodium Dodecyl Sulphate (SDS), 2% w/v DTE, 30% v/v glycerol and 0.05 M Tris-HCl pH 6.8, for 12 min; the second one composed of 6 M Urea, 2% w/v SDS, 2.5% w/v Iodoacetamide, 30% v/v glycerol, 0.05 M Tris-HCl pH 6.8 and a trace of bromophenol blue, for 5 min. The second dimension was then performed at 40 mA/gel constant current on 9-16% SDS polyacrylamide linear gradient gels (size: 18 x 20 cm x 1.5 mm) at 9°C. Analytical gels were stained with ammoniacal silver nitrate, while preparative gels underwent a mass spectrometry-compatible silver staining(128); then, gels were digitized with Image Scanner III laser densitometer supplied with the LabScan 6.0 software (GE Healthcare). 2D image analysis was performed using Melanie 9 software (Geneva Bioinformatics-GeneBio, Geneva, Swiss). Gel comparison highlighted quantitative and qualitative protein differences, validated by a statistical analysis. By Melanie 9 software, the ANOVA test was applied to compare the percentage of relative volume (%V) of the 2DE protein spots among the groups (ShC vs ShR). Particularly, only spots with a p-value ≤ 0.05 and a fold change at least of 1.5 in the %V means ratio, were considered differentially abundant.

Protein Identification by MALDI-ToF Mass Spectrometry

Differential proteins found were identified via MALDI-ToF MS using peptide mass fingerprinting (PMF). Differential spots were manually excised from MS-compatible silver-stained gels. Spots were destained first in a solution of 30 mM potassium ferricyanide and 100 mM sodium sulphate anhydrous, and then later in 200 mM ammonium bicarbonate. Then, they were dehydrated in 100% acetonitrile (ACN). Protein spots were rehydrated and digested overnight at 37 °C in a trypsin solution. Digested proteins were then placed on a MALDI target, dried, and covered with a matrix solution of 5 mg/mL α-cyano-4-hydroxycinnamic acid (CHCA) in 50% *v*/*v* ACN and 0.5% *v*/*v* trifluoroacetic acid (TFA). The MS analysis was carried out using the UltrafleXtreme™ MALDI-ToF/ToF mass spectrometer (Bruker Daltoniks, Bremen, Germany), equipped with a 200 Hz smartbeam™ I laser in the positive reflector mode with the following parameters: 80 ns of delay; ion source 1: 25 kV; ion source 2: 21.75 kV; lens voltage: 9.50 kV; reflector voltage: 26.30 kV; and reflector 2 voltage: 14.00 kV. The applied laser wavelength and frequency were 353 nm and 100 Hz, respectively, and the percentage was set to 50%. Final mass spectra were produced by

averaging 1500 laser shots targeting five different positions within the spot. MS spectra were acquired and processed via the FleXanalysis software version 3.0 (Bruker) using peptides arising from trypsin autoproteolysis as the internal standard for calibration. The resulting mass lists were filtered for common contaminants such as matrix-related ions, trypsin autolysis, and keratin peaks. Protein identification was carried out by utilizing the peptide mass fingerprinting search using MASCOT (Matrix Science Ltd., London, UK, http://www.matrixscience.com; accessed on 2 May 2022); setting up the following parameters: Homo sapiens as taxonomy, SwissProt as database, 20 ppm as mass tolerance, one admissible missed cleavage site, and carbamidomethylation (iodoacetamide alkylation) of cysteine as fixed modification and oxidation of methionine as a variable modification. Only protein identifications with a *p*-value < 0.04, a minimum of four matched peptides and a minimum MASCOT score of 55 were considered.

TCGA data download and pre-processing

TCGA SKCM data were downloaded through TCGAbiolinks(129). ENSEMBL gene Ids were converted to HGCN symbols with biomaRt(130), with the ENSEMBL ID having the highest average expression being kept in the case of multiple ENSEMBL IDs mapping to the same gene symbol, and data were log2 transformed with an offset of 1. Only samples annotated as metastatic were retained for further analyses.

Proteomic (RPPA) data were downloaded from the UCSC XENA database(131) and matched with the transcriptomic samples obtained from the corresponding patient.

All the TCGA data were downloaded in May 2021.

Correlation with survival

TCGA SKCM survival data were obtained with the GDCquery_clinic function from the TCGAbiolinks package. The overall survival of metastatic melanomas with the highest and lowest quartile in RICTOR/RAPTOR/MTOR expression were compared and displayed as Kaplan-Meier curves with the survminer package.

Enrichment analysis

Spearman's correlation between RICTOR and all other genes across metastatic melanomas (TCGA, transcriptional data) were obtained and ranked to perform a GSEA with Gene Ontology, Biological Process categories. For this, the msigdbr package(132) was used to obtain the GO lists (category C5, subcategory GO:BP) and the GSEA was done with the fgsea package(133).

Software and Plots

All the analyses were done with R 4.0.3(134).

Packages used for plotting: Ggpubr(134), survminer(135), ggplot2(136).

Statistical analysis

For statistical analyses, significance was tested with one-way ANOVA and two-way ANOVA, with Dunnett's, Sidak's or Tukey's *post hoc* tests. Statistical analysis was performed using the GraphPad Prism v8 software. $p < 0.05$ was considered significant. The definition of center and of dispersion and precision measures (e.g., mean and SD), as well as the number of technical or biological replicates of the experiments described and the specific statistical test used, are reported in the corresponding figure legends.

5. REFERENCES

1. Melanoma of the Skin — Cancer Stat Facts [Internet]. [cited 2024 Sep 21]. Available from: https://seer.cancer.gov/statfacts/html/melan.html

2. Evans MS, Madhunapantula SRV, Robertson GP, Drabick JJ. Current and future trials of targeted therapies in cutaneous melanoma. Adv Exp Med Biol. 2013;779:223–55.

3. Akbani R, Akdemir KC, Aksoy BA, Albert M, Ally A, Amin SB, et al. Genomic Classification of Cutaneous Melanoma. Cell. 2015 Jun 20;161(7):1681–96.

4. Dhomen N, Marais R. BRAF signaling and targeted therapies in melanoma. Hematol Oncol Clin North Am. 2009 Jun;23(3):529–45.

5. Wan PTC, Garnett MJ, Roe SM, Lee S, Niculescu-Duvaz D, Good VM, et al. Mechanism of activation of the RAF-ERK signaling pathway by oncogenic mutations of B-RAF. Cell. 2004 Mar 19;116(6):855–67.

6. Guo W, Wang H, Li C. Signal pathways of melanoma and targeted therapy. Signal Transduct Target Ther [Internet]. 2021 Dec 1 [cited 2024 Sep 21];6(1). Available from: https://pubmed.ncbi.nlm.nih.gov/34924562/

7. Haanen JB, Ascierto P, Larkin J, Dummer R, Garbe C, Testori A, et al. Improved Survival with Vemurafenib in Melanoma with BRAF V600E Mutation. 2011;2507–16.

8. Ascierto PA, Minor D, Ribas A, Lebbe C, O'Hagan A, Arya N, et al. Phase II trial (BREAK-2) of the BRAF inhibitor dabrafenib (GSK2118436) in patients with metastatic melanoma. J Clin Oncol Off J Am Soc Clin Oncol. 2013 Sep 10;31(26):3205–11.

9. Menzies AM, Long GV. Dabrafenib and trametinib, alone and in combination for BRAF-mutant metastatic melanoma. Clin Cancer Res Off J Am Assoc Cancer Res. 2014 Apr 15;20(8):2035–43.

10. https://www.esmo.org/oncology-news/archive/fda-approves-encorafenib-and-binimetinib-in-combination-for-unresectable-or-metastatic-melanoma-with-braf-mutations.

11. Vin H, Ojeda SS, Ching G, Leung ML, Chitsazzadeh V, Dwyer DW, et al. BRAF inhibitors suppress apoptosis through off-target inhibition of JNK signaling. eLife [Internet]. 2013 Nov 5 [cited 2024 Sep 21];2013(2). Available from: https://pubmed.ncbi.nlm.nih.gov/24192036/

12. Bromberger S, Zadorozhna Y, Ressler JM, Holzner S, Nawrocki A, Zila N, et al. Off-targets of BRAF inhibitors disrupt endothelial signaling and vascular barrier function. Life Sci Alliance [Internet]. 2024 Aug 1 [cited 2024 Sep 21];7(8). Available from: https://pubmed.ncbi.nlm.nih.gov/38839106/

13. Gibney GT, Messina JL, Fedorenko IV, Sondak VK, Smalley KSM. Paradoxical oncogenesis--the long-term effects of BRAF inhibition in melanoma. Nat Rev Clin Oncol. 2013 Jul;10(7):390–9.

14. Su F, Viros A, Milagre C, Trunzer K, Bollag G, Spleiss O, et al. RAS mutations in cutaneous squamous-cell carcinomas in patients treated with BRAF inhibitors. N Engl J Med. 2012 Jan 19;366(3):207–15.

15. Flaherty KT, Puzanov I, Kim KB, Ribas A, McArthur GA, Sosman JA, et al. Inhibition of mutated, activated BRAF in metastatic melanoma. N Engl J Med. 2010 Aug 26;363(9):809–19.

16. Tian Y, Guo W. A review of the molecular pathways involved in resistance to BRAF inhibitors in patients with advanced-stage melanoma. Med Sci Monit. 2020 Apr 10;26.

17. Tangella LP, Clark ME, Gray ES. Resistance mechanisms to targeted therapy in BRAF-mutant melanoma - A mini review. Biochim Biophys Acta - Gen Subj. 2021 Jan 1;1865(1).

18. What are Immune Checkpoint Inhibitors? Know Before Treatment | MD Anderson Cancer Center [Internet]. [cited 2024 Sep 22]. Available from: https://www.mdanderson.org/treatment-options/immune-checkpoint-inhibitors.html

19. Kichloo A, Albosta M, Dahiya D, Guidi JC, Aljadah M, Singh J, et al. Systemic adverse effects and toxicities associated with immunotherapy: A review. World J Clin Oncol. 2021 Mar 24;12(3):150.

20. Abdel-Wahab N, Alshawa A, Suarez-Almazor ME. Adverse Events in Cancer Immunotherapy. In: Naing A, Hajjar J, editors. Immunotherapy [Internet]. Cham: Springer International Publishing; 2017 [cited 2024 Oct 29]. p. 155–74. Available from: https://doi.org/10.1007/978-3-319-53156-4_8

21. Haas L, Elewaut A, Gerard CL, Umkehrer C, Leiendecker L, Pedersen M, et al. Acquired resistance to anti-MAPK targeted therapy confers an immune-evasive tumor microenvironment and cross-resistance to immunotherapy in melanoma. Nat Cancer. 2021 Jul;2(7):693–708.

22. Russo M, Chen M, Mariella E, Peng H, Rehman SK, Sancho E, et al. Cancer drug-tolerant persister cells: from biological questions to clinical opportunities. Nat Rev Cancer. 2024 Sep 2;

23. Catalanotti F, Cheng DT, Shoushtari AN, Johnson DB, Panageas KS, Momtaz P, et al. PTEN Loss-of-Function Alterations Are Associated With Intrinsic Resistance to BRAF Inhibitors in Metastatic Melanoma. JCO Precis Oncol. 2017;1.

24. Cabrita R, Mitra S, Sanna A, Ekedahl H, Lövgren K, Olsson H, et al. The Role of PTEN Loss in Immune Escape, Melanoma Prognosis and Therapy Response. Cancers. 2020 Mar 21;12(3).

25. Gibney GT, Smalley KSM, Affi ', Corresponding F, Lee Moffi H. An Unholy Alliance: Cooperation between BRAF and NF1 in Melanoma Development and BRAF Inhibitor Resistance. Cancer Discov. 2013 Mar 1;3(3):260–3.

26. Whittaker SR, Theurillat JP, Van Allen E, Wagle N, Hsiao J, Cowley GS, et al. A genome-scale RNA interference screen implicates NF1 loss in resistance to RAF inhibition. Cancer Discov. 2013 Mar;3(3):350–62.

27. Shalem O, Sanjana NE, Hartenian E, Shi X, Scott DA, Mikkelson T, et al. Genome-scale CRISPR-Cas9 knockout screening in human cells. Science. 2014 Jan 3;343(6166):84–7.

28. Smalley KSM, Lioni M, Dalla Palma M, Xiao M, Desai B, Egyhazi S, et al. Increased cyclin D1 expression can mediate BRAF inhibitor resistance in BRAF V600E-mutated melanomas. Mol Cancer Ther. 2008 Sep;7(9):2876–83.

29. Krauthammer M, Kong Y, Ha BH, Evans P, Bacchiocchi A, McCusker JP, et al. Exome sequencing identifies recurrent somatic RAC1 mutations in melanoma. Nat Genet. 2012 Sep;44(9):1006–14.

30. Hodis E, Watson IR, Kryukov GV, Arold ST, Imielinski M, Theurillat JP, et al. A landscape of driver mutations in melanoma. Cell. 2012 Jul 20;150(2):251–63.

31. Müller J, Krijgsman O, Tsoi J, Robert L, Hugo W, Song C, et al. Low MITF/AXL ratio predicts early resistance to multiple targeted drugs in melanoma. Nat Commun. 2014 Dec 15;5.

32. Carotenuto P, Romano A, Barbato A, Quadrano P, Brillante S, Volpe M, et al. Targeting the MITF/APAF-1 axis as salvage therapy for MAPK inhibitors in resistant melanoma. Cell Rep. 2022 Nov 8;41(6).

33. Ji Z, Erin Chen Y, Kumar R, Taylor M, Jenny Njauw CN, Miao B, et al. MITF modulates therapeutic resistance through EGFR signaling. J Invest Dermatol. 2015 Jul 18;135(7):1863–72.

34. Hanahan D. Hallmarks of Cancer: New Dimensions. Cancer Discov. 2022 Jan;12(1):31–46.

35. Cantor JR, Sabatini DM. Cancer cell metabolism: one hallmark, many faces. Cancer Discov. 2012 Oct;2(10):881–98.

36. Faubert B, Solmonson A, DeBerardinis RJ. Metabolic reprogramming and cancer progression. Science. 2020 Apr 10;368(6487).

37. Chang CH, Qiu J, O'Sullivan D, Buck MD, Noguchi T, Curtis JD, et al. Metabolic Competition in the Tumor Microenvironment Is a Driver of Cancer Progression. Cell. 2015 Sep 10;162(6):1229–41.

38. DeBerardinis RJ, Chandel NS. Fundamentals of cancer metabolism. Sci Adv. 2016 May;2(5):e1600200.

39. Allison KE, Coomber BL, Bridle BW. Metabolic reprogramming in the tumour microenvironment: a hallmark shared by cancer cells and T lymphocytes. Immunology. 2017 Oct;152(2):175–84.

40. Warburg O, Wind F, Negelein E. THE METABOLISM OF TUMORS IN THE BODY. J Gen Physiol. 1927 Mar 7;8(6):519–30.

41. Zheng J. Energy metabolism of cancer: Glycolysis versus oxidative phosphorylation (Review). Oncol Lett. 2012 Dec;4(6):1151–7.

42. Abildgaard C, Guldberg P. Molecular drivers of cellular metabolic reprogramming in melanoma. Trends Mol Med. 2015 Mar;21(3):164–71.

43. Porporato PE, Filigheddu N, Pedro JMBS, Kroemer G, Galluzzi L. Mitochondrial metabolism and cancer. Cell Res. 2018 Mar;28(3):265–80.

44. Vyas S, Zaganjor E, Haigis MC. Mitochondria and Cancer. Cell. 2016 Jul 28;166(3):555–66.

45. Sabharwal SS, Schumacker PT. Mitochondrial ROS in cancer: initiators, amplifiers or an Achilles' heel? Nat Rev Cancer. 2014 Nov;14(11):709–21.

46. Harel M, Ortenberg R, Varanasi SK, Mangalhara KC, Mardamshina M, Markovits E, et al. Proteomics of Melanoma Response to Immunotherapy Reveals Mitochondrial Dependence. Cell. 2019 Sep 19;179(1):236-250.e18.

47. Avagliano A, Fiume G, Pelagalli A, Sanità G, Ruocco MR, Montagnani S, et al. Metabolic Plasticity of Melanoma Cells and Their Crosstalk With Tumor Microenvironment. Front Oncol. 2020;10:722.

48. Scott DA, Richardson AD, Filipp FV, Knutzen CA, Chiang GG, Ronai ZA, et al. Comparative metabolic flux profiling of melanoma cell lines: beyond the Warburg effect. J Biol Chem. 2011 Dec 9;286(49):42626–34.

49. Romero-Garcia S, Moreno-Altamirano MMB, Prado-Garcia H, Sánchez-García FJ. Lactate Contribution to the Tumor Microenvironment: Mechanisms, Effects on Immune Cells and Therapeutic Relevance. Front Immunol. 2016;7:52.

50. Denko NC. Hypoxia, HIF1 and glucose metabolism in the solid tumour. Nat Rev Cancer. 2008 Sep;8(9):705–13.

51. Vazquez F, Lim JH, Chim H, Bhalla K, Girnun G, Pierce K, et al. PGC1α expression defines a subset of human melanoma tumors with increased mitochondrial capacity and resistance to oxidative stress. Cancer Cell. 2013 Mar 18;23(3):287–301.

52. Haq R, Shoag J, Andreu-Perez P, Yokoyama S, Edelman H, Rowe GC, et al. Oncogenic BRAF regulates oxidative metabolism via PGC1α and MITF. Cancer Cell. 2013 Mar 18;23(3):302–15.

53. Audrito V, Managò A, Gaudino F, Deaglio S. Targeting metabolic reprogramming in metastatic melanoma: The key role of nicotinamide phosphoribosyltransferase (NAMPT). Semin Cell Dev Biol. 2020;98(March):192–201.

54. Parmenter TJ, Kleinschmidt M, Kinross KM, Bond ST, Li J, Kaadige MR, et al. Response of BRAF-mutant melanoma to BRAF inhibition is mediated by a network of transcriptional regulators of glycolysis. Cancer Discov. 2014 Apr;4(4):423–33.

55. Corazao-Rozas P, Guerreschi P, Jendoubi M, André F, Jonneaux A, Scalbert C, et al. Mitochondrial oxidative stress is the achille's heel of melanoma cells resistant to Braf-mutant inhibitor. Oncotarget. 2013;4(11):1986–98.

56. Jia D, Park JH, Jung KH, Levine H, Kaipparettu BA. Elucidating the Metabolic Plasticity of Cancer: Mitochondrial Reprogramming and Hybrid Metabolic States. Cells. 2018 Mar 13;7(3).

57. Chiarugi A, Dölle C, Felici R, Ziegler M. The NAD metabolome--a key determinant of cancer cell biology. Nat Rev Cancer. 2012 Nov;12(11):741–52.

58. Xie N, Zhang L, Gao W, Huang C, Huber PE, Zhou X, et al. NAD(+) metabolism: pathophysiologic mechanisms and therapeutic potential. Signal Transduct Target Ther. 2020 Oct 7;5(1):227.

59. Audrito V, Messana VG, Brandimarte L, Deaglio S. The Extracellular NADome Modulates Immune Responses. Front Immunol. 2021;12:704779.

60. Heske CM. Beyond Energy Metabolism: Exploiting the Additional Roles of NAMPT for Cancer Therapy. Front Oncol. 2019;9:1514.

61. Audrito V, Messana VG, Deaglio S. NAMPT and NAPRT: Two Metabolic Enzymes With Key Roles in Inflammation. Front Oncol. 2020;10:358.

62. Garten A, Schuster S, Penke M, Gorski T, de Giorgis T, Kiess W. Physiological and pathophysiological roles of NAMPT and NAD metabolism. Nat Rev Endocrinol. 2015 Sep;11(9):535–46.

63. Kim D hyung, Sarbassov DD, Ali SM, Latek RR, Guntur KVP, Erdjument-bromage H, et al. GbetaL , a Positive Regulator of the Rapamycin- Sensitive Pathway Required for the Nutrient- Sensitive Interaction between Raptor and mTOR. 2003;11:895–904.

64. Peterson TR, Laplante M, Thoreen CC, Sancak Y, Kang SA, Kuehl WM, et al. DEPTOR Is an mTOR Inhibitor Frequently Overexpressed in Multiple Myeloma Cells and Required for Their Survival. Cell. 2009;137(5):873–86.

65. Haar EV, Lee S il, Bandhakavi S, Griffin TJ, Kim D hyung. Insulin signalling to mTOR mediated by the Akt / PKB substrate PRAS40. 2007;9(3).

66. Sancak Y, Peterson TR, Shaul YD, Lindquist RA, Thoreen CC, Bar-peled L, et al. The Rag GTPases Bind Raptor and Mediate Amino Acid Signaling to mTORC1. 2008;(June):1496–502.

67. Hay N. Interplay between FOXO, TOR, and Akt. Biochim Biophys Acta. 2011 Nov;1813(11):1965–70.

68. Liu GY. mTOR at the nexus of nutrition, growth, ageing and disease. Nat Rev Mol Cell Biol [Internet]. 2020;8. Available from: http://dx.doi.org/10.1038/s41580-019-0199-y

69. Garc JM, Alessi DR. Activation of serum- and glucocorticoid-induced protein kinase 1 (SGK1). 2008;385:375–85.

70. Ikenoue T, Inoki K, Yang Q, Zhou X, Guan K liang. Essential function of TORC2 in PKC and Akt turn motif phosphorylation , maturation and signalling. 2008;27(14):1919–31.

71. Ebner M, Sinkovics B, Szczygie M, Ribeiro DW, Yudushkin I. Localization of mTORC2 activity inside cells. 216(2):343–53.

72. Humphrey SJ, Yang G, Yang P, Fazakerley DJ, Stöckli J, Yang JY, et al. Dynamic adipocyte phosphoproteome reveals that Akt directly regulates mTORC2. Cell Metab. 2013 Jun 4;17(6):1009–20.

73. Knudsen JR, Fritzen AM, James DE, Jensen TE, Kleinert M, Richter EA. Growth Factor-Dependent and -Independent Activation of mTORC2. Trends Endocrinol Metab. 2019;1–12.

74. Dhomen N, Reis-Filho JS, da Rocha Dias S, Hayward R, Savage K, Delmas V, et al. Oncogenic Braf induces melanocyte senescence and melanoma in mice. Cancer Cell. 2009 Apr 7;15(4):294–303.

75. Goel VK, Ibrahim N, Jiang G, Singhal M, Fee S, Flotte T, et al. Melanocytic nevus-like hyperplasia and melanoma in transgenic BRAFV600E mice. Oncogene. 2009 Jun 11;28(23):2289–98.

76. Damsky W, Micevic G, Meeth K, Muthusamy V, Curley DP, Santhanakrishnan M, et al. mTORC1 activation blocks brafV600E-induced growth arrest but is insufficient for melanoma formation. Cancer Cell. 2015;27(1):41–56.

77. Sun Y, Li R, Nong B, Songyang Z, Wang X, Ma W, et al. A Comprehensive Pan-Cancer Analysis of the Potential Biological Functions and Prognosis Values of RICTOR. Genes. 2023 Jun 16;14(6):1280.

78. Colombi M, Molle KD, Benjamin D, Rattenbacher-Kiser K, Schaefer C, Betz C, et al. Genome-wide shRNA screen reveals increased mitochondrial dependence upon mTORC2 addiction. Oncogene. 2011 Mar 31;30(13):1551–65.

79. Mossmann D, Park S, Hall MN. mTOR signalling and cellular metabolism are mutual determinants in cancer. Nat Rev Cancer. 2018 Dec;18(12):744–57.

80. Lamming DW, Demirkan G, Boylan JM, Mihaylova MM, Peng T, Ferreira J, et al. Hepatic signaling by the mechanistic target of rapamycin complex 2 (mTORC2). FASEB J. 2014;28(1):300–15.

81. Morita M, Gravel SP, Chénard V, Sikström K, Zheng L, Alain T, et al. mTORC1 controls mitochondrial activity and biogenesis through 4E-BP-dependent translational regulation. Cell Metab. 2013 Nov 5;18(5):698–711.

82. Kim CS, Ding X, Allmeroth K, Biggs LC, Kolenc OI, L'Hoest N, et al. Glutamine Metabolism Controls Stem Cell Fate Reversibility and Long-Term Maintenance in the Hair Follicle. Cell Metab. 2020 Oct 6;32(4):629-642.e8.

83. Tassone B, Saoncella S, Neri F, Ala U, Brusa D, Magnuson MA, et al. Rictor / mTORC2 deficiency enhances keratinocyte stress tolerance via mitohormesis. 2017;731–46.

84. Yang Q, Inoki K, Ikenoue T, Guan KL. Identification of Sin1 as an essential TORC2 component required for complex formation and kinase activity. Genes Dev. 2006 Oct 15;20(20):2820–32.

85. Yoon S oh, Shin S, Karreth FA, Roux PP, Dephoure N, Blenis J, et al. Focal Adhesion- and IGF1R-Dependent Survival and Migratory Pathways Mediate Tumor Resistance to Focal Adhesion- and IGF1R-Dependent Survival and Migratory Pathways Mediate Tumor Resistance to mTORC1 / 2 Inhibition. Mol Cell. 2017;67(3):512-527.e4.

86. Xie X, Zhang D, Zhao B, Lu M kan, You M, Condorelli G, et al. I κ B kinase ε and TANK-binding kinase 1 activate AKT by direct phosphorylation. 2011;

87. Resistance P, Stronach EA, Chen M, Maginn EN, Agarwal R, Mills GB, et al. DNA-PK Mediates AKT Activation and Apoptosis Inhibition in Clinically Acquired. 2011;13(11):1069–80.

88. Mahajan K, Mahajan NP. PI3K-independent AKT activation in cancers: A treasure trove for novel therapeutics. J Cell Physiol. 2012 Sep;227(9):3178–84.

89. Capparelli C, Purwin TJ, Glasheen MK, Caksa S, Tiago M, Wilski N, et al. Targeting SOX10-deficient cells to reduce the dormant-invasive phenotype state in melanoma. Nat Commun. 2022 Dec 1;13(1).

90. Sun C, Wang L, Huang S, Heynen GJJE, Prahallad A, Robert C, et al. Reversible and adaptive resistance to BRAF(V600E) inhibition in melanoma. Nature. 2014;508(1):118–22.

91. Wang L, Leite de Oliveira R, Huijberts S, Bosdriesz E, Pencheva N, Brunen D, et al. An Acquired Vulnerability of Drug-Resistant Melanoma with Therapeutic Potential. Cell. 2018 May 31;173(6):1413-1425.e14.

92. Yang C, Tian C, Hoffman TE, Jacobsen NK, Spencer SL. Melanoma subpopulations that rapidly escape MAPK pathway inhibition incur DNA damage and rely on stress signalling. Nat Commun. 2021 Dec 1;12(1).

93. Wang F, Zhang D, Zhang D, Li P, Gao Y. Mitochondrial Protein Translation: Emerging Roles and Clinical Significance in Disease. Front Cell Dev Biol. 2021 Jul 1;9.

94. Gowthami N, Sunitha B, Kumar M, Keshava Prasad TS, Gayathri N, Padmanabhan B, et al. Mapping the protein phosphorylation sites in human mitochondrial complex I (NADH: Ubiquinone oxidoreductase): A bioinformatics study with implications for brain aging and neurodegeneration. J Chem Neuroanat. 2019 Jan 1;95:13–28.

95. Srinivas Bharath MM. Post-Translational Oxidative Modifications of Mitochondrial Complex i (NADH: Ubiquinone Oxidoreductase): Implications for Pathogenesis and Therapeutics in Human Diseases. J Alzheimers Dis. 2017;60(s1):S69–86.

96. Shinmura K, Tamaki K, Sano M, Nakashima-Kamimura N, Wolf AM, Amo T, et al. Caloric restriction primes mitochondria for ischemic stress by deacetylating specific mitochondrial proteins of the electron transport chain. Circ Res. 2011 Aug 5;109(4):396–406.

97. Sociali G, Grozio A, Caffa I, Schuster S, Becherini P, Damonte P, et al. SIRT6 deacetylase activity regulates NAMPT activity and NAD(P)(H) pools in cancer cells. FASEB J Off Publ Fed Am Soc Exp Biol. 2019;33(3):3704–17.

98. Liao X, Huang X, Li X, Qiu X, Li M, Liu R, et al. AMPK phosphorylates NAMPT to regulate NAD(+) homeostasis under ionizing radiation. Open Biol. 2022 Oct;12(10):220213.

99. Lin J, Chen K, Chen W, Yao Y, Ni S, Ye M, et al. Paradoxical Mitophagy Regulation by PINK1 and TUFm. Mol Cell. 2020 Nov 19;80(4):607-620.e12.

100. Qi B, Song L, Hu L, Guo D, Ren G, Peng T, et al. Cardiac-specific overexpression of Ndufs1 ameliorates cardiac dysfunction after myocardial infarction by alleviating mitochondrial dysfunction and apoptosis. Exp Mol Med. 2022 Jul 1;54(7):946–60.

101. Liu N, Pang B, Kang L, Li D, Jiang X, Zhou CM. TUFM in health and disease: exploring its multifaceted roles. Front Immunol. 2024;15:1424385.

102. Yendapally R, Sikazwe D, Kim SS, Ramsinghani S, Fraser-Spears R, Witte AP, et al. A review of phenformin, metformin, and imeglimin. Drug Dev Res. 2020 Jun 1;81(4):390–401.

103. Bertolotto C, Ohanna M, Ballotti R. Key role of nicotinamide phosphoribosyltransferase (NAMPT) and NAD metabolism in the transition of melanoma cells to an invasive and drug-resistant phenotype. Medecine/Sciences. 2018;34(12):1025–8.

104. Guertin DA, Stevens DM, Saitoh M, Kinkel S, Crosby K, Sheen J ho, et al. mTOR Complex 2 Is Required for the Development of Prostate Cancer Induced by Pten Loss in Mice. Cancer Cell. 2009;15(2):148–59.

105. Kim LC, Cook RS, Chen J. MTORC1 and mTORC2 in cancer and the tumor microenvironment. Oncogene. 2017 Apr 20;36(16):2191–201.

106. Schmidt KM, Dietrich P, Hackl C, Guenzle J, Bronsert P, Wagner C, et al. Inhibition of mTORC2/RICTOR Impairs Melanoma Hepatic Metastasis. Neoplasia U S. 2018 Dec 1;20(12):1198–208.

107. Jebali A, Battistella M, Lebbé C, Dumaz N. Rictor affects melanoma tumorigenesis and its resistance to targeted therapy. Biomedicines. 2021 Oct 1;9(10).

108. Akgül S, Li Y, Zheng S, Kool M, Treisman DM, Li C, et al. Opposing Tumor-Promoting and -Suppressive Functions of Rictor/mTORC2 Signaling in Adult Glioma and Pediatric SHH Medulloblastoma. Cell Rep. 2018;24(2):463-478.e5.

109. Gu Y, Albuquerque CP, Braas D, Zhang W, Villa GR, Bi J, et al. mTORC2 Regulates Amino Acid Metabolism in Cancer by Phosphorylation of the Cystine-Glutamate Antiporter xCT. Mol Cell. 2017;67(1):128-138.e7.

110. Luciano AK, Korobkina ED, Lyons SP, Haley JA, Fluharty SM, Jung SM, et al. Proximity labeling of endogenous RICTOR identifies mTOR complex 2 regulation by ADP ribosylation factor ARF1. J Biol Chem. 2022 Oct 1;298(10).

111. Koo J, Wu X, Mao Z, Khuri FR, Sun SY. Rictor undergoes glycogen synthase kinase 3 (GSK3)-dependent, FBXW7-mediated ubiquitination and proteasomal degradation. J Biol Chem. 2015 May 29;290(22):14120–9.

112. Sane S, Srinivasan R, Potts RA, Eikanger M, Zagirova D, Freeling J, et al. UBXN2A suppresses the Rictor-mTORC2 signaling pathway, an established tumorigenic pathway in human colorectal cancer. Oncogene. 2023 May 22;42(21):1763–76.

113. Pergolizzi B, Panuzzo C, Shahzad Ali M, Iacono ML, Levron CL, Ponzone L, et al. Two conserved glycine residues in mammalian and Dictyostelium Rictor are required for mTORC2 activity and integrity. J Cell Sci. 2019;132(22).

114. Shen S, Vagner S, Robert C. Persistent Cancer Cells: The Deadly Survivors. Cell. 2020 Nov 12;183(4):860–74.

115. Ghafouri-Fard S, Gholipour M, Taheri M. MicroRNA Signature in Melanoma: Biomarkers and Therapeutic Targets. Front Oncol. 2021 Apr 22;11.

116. Micevic G, Muthusamy V, Damsky W, Theodosakis N, Liu X, Meeth K, et al. DNMT3b Modulates Melanoma Growth by Controlling Levels of mTORC2 Component RICTOR. Cell Rep. 2016 Mar 8;14(9):2180–92.

117. Shen W, Zhou Q, Peng C, Li J, Yuan Q, Zhu H, et al. FBXW7 and the Hallmarks of Cancer: Underlying Mechanisms and Prospective Strategies. Front Oncol. 2022;12:880077.

118. Qin S, Wang G, Chen L, Geng H, Zheng Y, Xia C, et al. Pharmacological vitamin C inhibits mTOR signaling and tumor growth by degrading Rictor and inducing HMOX1 expression. PLoS Genet. 2023 Feb 14;19(2).

119. Ji S, Qin Y, Shi S, Liu X, Hu H, Zhou H, et al. ERK kinase phosphorylates and destabilizes the tumor suppressor FBW7 in pancreatic cancer. Cell Res. 2015 May;25(5):561–73.

120. Hung CM, Calejman CM, Sanchez-Gurmaches J, Li H, Clish CB, Hettmer S, et al. Rictor/mTORC2 loss in the Myf5 lineage reprograms brown fat metabolism and protects mice against obesity and metabolic disease. Cell Rep. 2014 Jul 10;8(1):256–71.

121. Entwisle SW, Calejman CM, Valente AS, Lawrence RT, Hung CM, Guertin DA, et al. Proteome and phosphoproteome analysis of brown adipocytes reveals that RICTOR loss dampens global insulin/AKT signaling. Mol Cell Proteomics. 2020 Jul 1;19(7):1104–19.

122. Greger JG, Eastman SD, Zhang V, Bleam MR, Hughes AM, Smitheman KN, et al. Combinations of BRAF, MEK, and PI3K/mTOR inhibitors overcome acquired resistance to the BRAF inhibitor GSK2118436 dabrafenib, mediated by NRAS or MEK mutations. Mol Cancer Ther. 2012;11(4):909–20.

123. Lv H, Lv G, Chen C, Zong Q, Jiang G, Ye D, et al. NAD+ Metabolism Maintains Inducible PD-L1 Expression to Drive Tumor Immune Evasion. Cell Metab. 2021 Jan 5;33(1):110-127.e5.

124. Chandra Mangalhara K, Karthik Varanasi S, Johnson MA, Burns MJ, Rojas GR, Esparza Moltó PB, et al. Manipulating mitochondrial electron flow enhances tumor immunogenicity [Internet]. Available from: https://www.science.org

125. Saoncella S, Tassone B, Deklic E, Avolio F, Jon C, Tornillo G, et al. Nuclear Akt2 opposes limbal keratinocyte stem cell self-renewal by repressing a FOXO-mTORC1 signaling pathway. Stem Cells. 2014 Mar;32(3):754–69.

126. Zamporlini F, Ruggieri S, Mazzola F, Amici A, Orsomando G, Raffaelli N. Novel assay for simultaneous measurement of pyridine mononucleotides synthesizing activities allows dissection of the NAD + biosynthetic machinery in mammalian cells. FEBS J. 2014 Nov 1;281(22):5104–19.

127. Landi C, Liberatori G, Puccini M, Shaba E, Vantaggiato L, Vitolo S, et al. Proteomics coupled with AhR-reporter gene bioassay for human and environmental safety assessment of sewage sludge and hydrochar. Sci Total Environ. 2023 Sep 15;891.

128. Chevallet M, Luche S, Diemer H, Strub JM, Van Dorsselaer A, Rabilloud T. Sweet silver: A formaldehyde-free silver staining using aldoses as developing agents, with enhanced compatibility with mass spectrometry. Proteomics. 2008;8(23–24):4853–61.

129. Colaprico A, Silva TC, Olsen C, Garofano L, Cava C, Garolini D, et al. TCGAbiolinks: An R/Bioconductor package for integrative analysis of TCGA data. Nucleic Acids Res. 2016 May 5;44(8):e71.

130. Durinck S, Spellman PT, Birney E, Huber W. Mapping identifiers for the integration of genomic datasets with the R/ Bioconductor package biomaRt. Nat Protoc. 2009;4(8):1184–91.

131. Goldman MJ, Craft B, Hastie M, Repečka K, McDade F, Kamath A, et al. Visualizing and interpreting cancer genomics data via the Xena platform. Nat Biotechnol. 2020 Jun 1;38(6):675–8.

132. Dolgalev I. msigdbr: MSigDB Gene Sets for Multiple Organisms in a Tidy Data Format. R package version 7.1.1. https://CRAN.R-project.org/package=msigdbr. 2020;

133. Korotkevich G, Sukhov V, Budin N, Shpak B, Artyomov MN, Sergushichev A. Fast gene set enrichment analysis. Available from: https://doi.org/10.1101/060012

134. Kassambara A. Ggpubr:“Ggplot2” Based Publication Ready Plots (Version 0.3. 0)[Computer Software]. 2020;

135. Kassambara A, Kosinski M, Biecek P. survminer: Drawing Survival Curves using “ggplot2”. R package version 0.4.8. https://CRAN.R-project.org/package=survminer. 2020;

136. Gómez-Rubio V. ggplot2 - Elegant Graphics for Data Analysis (2nd Edition). J Stat Softw. 2017;77(Book Review 2).